

Density-Functional Theory (DFT) and Time-Dependent DFT Study of the Chemical and Physical Origins of Key Photoproperties of End-Group Derivatives of the Nonfullerene Bulk Heterojunction Organic Solar Cell Acceptor Molecule IDIC

Taouali W*, Alimi K*, Nangraj A.S. †, Casida M.E. ‡

Abstract

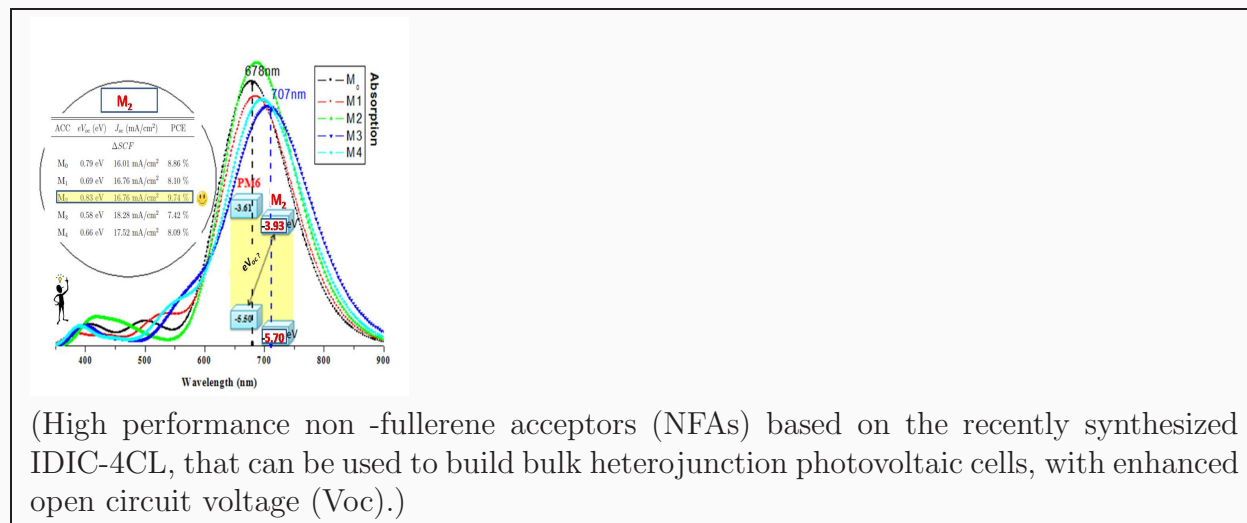
As emphasized in a recent review article [*Chem. Rev.* **122**, 14180 (2022)], organic solar cell (OSC) photoconversion efficiency has been rapidly evolving with results increasingly comparable to those of traditional inorganic solar cells. Historically, OSC performance improvement focused first on the morphology of P3HT:PC₆₁BM solar cells then went through different stages to shift lately interest towards non-fullerene acceptors (NFAs) as a replacement of PC₆₁BM acceptor (ACC) molecule. Here, we use density-functional theory (DFT) and time-dependent (TD) DFT to investigate four novel NFAs of A-D-A (acceptor-donor-acceptor) form derived from the recently synthesized IDIC-4Cl [*Dyes and Pigments* **166**, 196 (2019)]. Our level of theory is carefully evaluated for IDIC-4Cl and then applied to the four novel NFAs in order to understand how chemical modifications lead to physical changes in cyclic voltammetry (CV) frontier molecular orbital (FMO) energies and absorption spectra in solution. Finally we design and apply a new type of Scharber plot for NFAs based upon some simple but we think reasonable assumptions. Unlike the original Scharber plots where a larger DON band gap favors a larger PCE, our modified Scharber plot reflects the fact that a smaller ACC band gap may favor PCE by filling in gaps in the DON acceptor spectrum. We predict that only the candidate molecule with the *least* good acceptor A, with the *highest* frontier molecular orbital energies, and *one of the larger* CV lowest unoccupied molecular orbital (LUMO) – highest unoccupied molecular orbital (HOMO) gaps, will yield a PM6:ACC PCE exceeding that of the parent IDIC-4Cl ACC. This candidate also shows the largest oscillator strength for the primary ¹(HOMO,LUMO) charge- transfer transition and the largest degree of delocalization of charge transfer of any of the ACC molecules investigated here.

*Laboratoire de Recherche (LR18ES19), Synthèse Asymétrique et Ingénierie Moléculaire de Matériaux Organiques pour l'Électroniques Organiques, Faculté des Sciences de Monastir, Université de Monastir, 5000 Monastir, TUNISIA

†State Key Laboratory of Microbial Metabolism, Shanghai Jiao Tong University, Shanghai, CHINA

‡Laboratoire de Spectrométrie, Interactions et Chimie théorique (SITh), Département de Chimie Moléculaire (DCM, UMR CNRS/UGA 5250), Institut de Chimie Moléculaire de Grenoble (ICMG, FR2607), Université Grenoble Alpes (UGA) 301 rue de la Chimie, BP 53, F-38041 Grenoble Cedex 9, FRANCE

Keywords: density-functional theory, time-dependent density-functional theory, transition density matrix , organic solar cell, nonfullerene acceptors. ■



(High performance non -fullerene acceptors (NFAs) based on the recently synthesized IDIC-4CL, that can be used to build bulk heterojunction photovoltaic cells, with enhanced open circuit voltage (Voc).)

1 Introduction

Organic electronics has emerged as competitive with silicon-based electronics for many applications. Reasons for this include ease of manufacture and the possibility of printing of circuit components, as well as the ability to use the principles of organic chemistry to design the materials used in organic electronic devices at the molecular level. One particularly prominent example of organic electronics is the increasingly wide spread use in displays of organic light emitting diodes. Another is the rapid emergence of organic solar cells (OSCs). Once limited to niche markets because of low photoconversion efficiencies (PCE), OSCs now have experimental PCEs as high as 18%¹⁻³ with 20% PCE expected in the near future⁴. The typical modern OSC is of the DON:ACC bulk heterojunction type where a donor material (DON) is mixed with an acceptor (ACC) material in an immiscible mixture. Phase separation causes a dramatic increase in the surface area of the DON:ACC heterojunction. Such an OSC is a complex system, the modeling of which would have to take into account a wide range of time scales from femtoseconds to microseconds and length scales from nanometers to centimeters and would have to include structural details as well as exciton and charge transfer rates whose modeling is not yet sufficiently well understood. Much less ambitious, but still challenging, is to take an experimentally characterized DON:ACC OSC and try to predict how chemical modifications will affect the OSC PCE. To this end, we have chosen to study a third generation nonfullerene acceptor (NFA) of the A-D-A form where A is an electron accepting group and D is an electron donating group. In particular, IDIC-4Cl is well characterized with a PM6:IDIC-4Cl PCE of about 10%. Changing the Cl end groups is likely to have little effect other than on the absorption spectrum and the highest occupied molecular orbital (HOMO) and lowest unoccupied orbital (LUMO) energies. These frontier molecular orbital (FMO) energies are measured by cyclic voltammetry (CV) and hence must be calculated as the appropriate oxidation and reduction potentials. Finally these must be combined with other data to see how varying electron donating and accepting groups in the A-D-A acceptor affect the DON:ACC OSC PCE. The molecules studied here are shown in **Fig. 1**. Our approach is a first principles one using density-functional theory (DFT) and time-dependent (TD) DFT. This allows us to obtain a detailed picture of how molecular-level modifications may change OSC performance at the macroscopic level.

OSC

PCE

DON,
ACC

NFA

A, D
HOMO,
LUMO,
FMO
CV

DFT,
TD

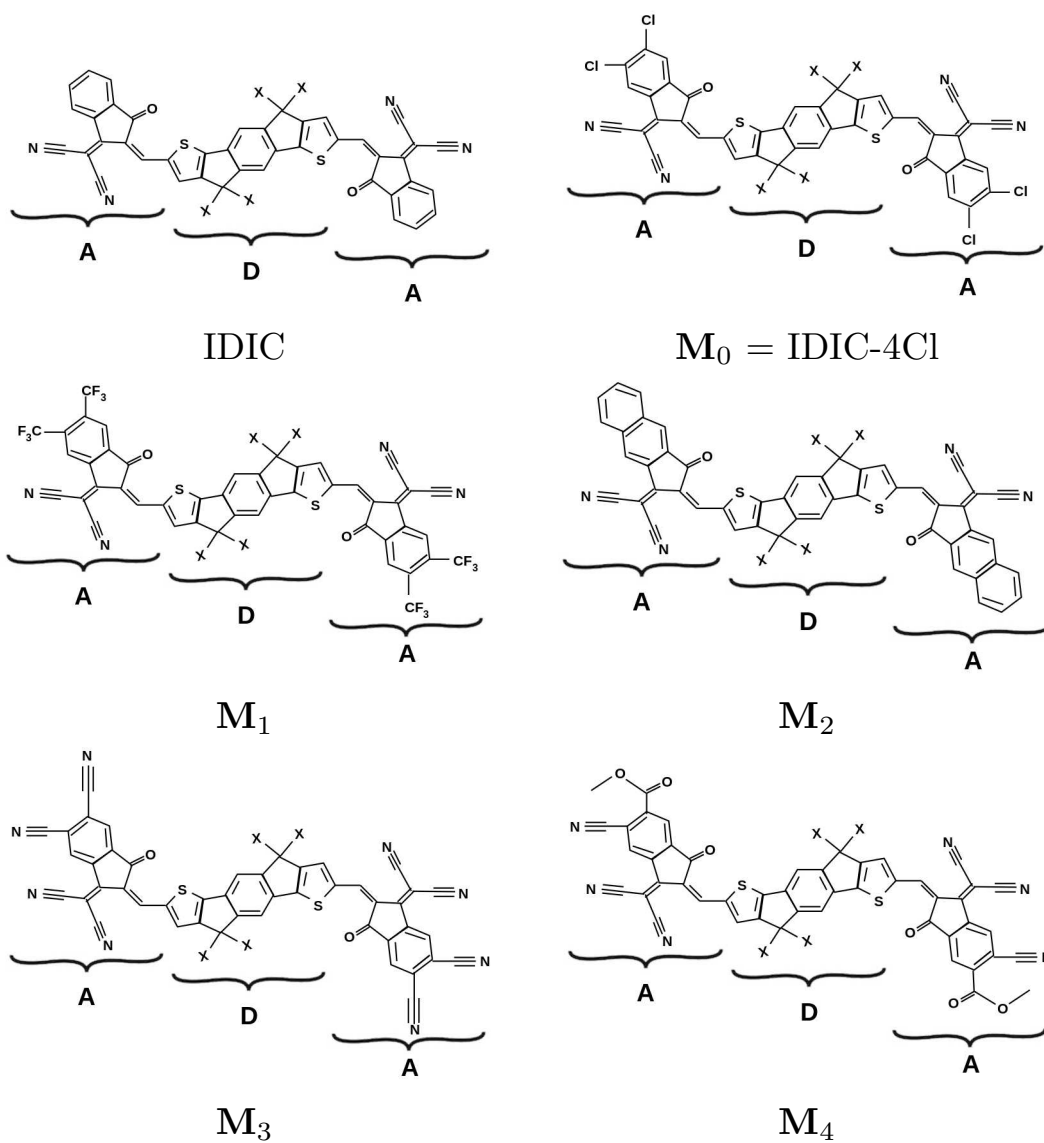


Figure 1: The chemical structures of IDIC and the non-fullerene ACC (NFAs) treated in this article. In our work X is a methyl group, but in the literature X is typically an *n*-hexyl or *n*-octyl group. See the Supplementary Information.

The reader is referred to a recent review covering the rapid development of OSCs that has taken place over the last two decades⁴. That review divides the evolution of DON:ACC OSCs into three main stages or generations. During the first generation, typical OSCs were of the P3HT:PC₆₁BM type where P3HT is a conducting polymer donor and PC₆₁BM is buckminsterfullerene with an added substituent to improve solubility and hence ease of manipulation. The main emphasis during the first generation was on optimizing the PCE through optimization of the morphology of the bulk heterojunction.

The second generation consisted of replacing P3HT with other DON polymers. First principles modeling of OSC PCEs is not discussed very much in the recent review⁴. Here we just mention that the PCE is usually determined by using the Shockley diode model and measuring the short-circuit current density J_{sc} , open-circuit voltage V_{oc} , and fill factor (FF), from which the PCE may be calculated. Note however that the Shockley diode theory was developed for inorganic devices and that the parameters entering into the theory may need to be reinterpreted for organic devices^{5,6}, nor can this theory describe the S-shaped current-voltage curves sometimes observed for OSCs⁵⁻⁸. Moreover modeling exciton and charge transfer requires deciding whether conduction is band-like or by hopping, when real organic systems often have elements of both^{9,10}. In principle, electron and hole mobilities, the absorption spectra of both the DON and ACC phases, as the thickness of the layers, are needed to correctly model the relation between photoabsorption and photoconductivity spectra¹¹⁻¹⁴. And there is the possibility that heterojunction surface states may also alter photoabsorption and photoconductivity spectra¹². It was therefore fortunate that photon absorption and the associated exciton formation occurred primarily in the ACC material in second generation OSCs, allowing Scharber to propose a relatively simple partially phenomenological and partly detailed balance model for predicting OSC PCEs^{15,16} [see the Supplementary Information (SI) for the present article].

The third generation is characterized by optimizing the ACC in the DON:ACC OSC. Great success was found with small molecule NFAs^{4,17-20}, many with the A-D-A configuration²¹⁻²⁴. The greatest advantages of these NFAs over fullerenes are the complementary donor/acceptor photoabsorption, improved solubility, local crystallinity, and tunability of their optoelectronic properties²⁵⁻²⁷. These molecules tend to be relatively flat with a large fused-ring D and strong electron withdrawing units. Their flatness allows them to stack, forming locally crystalline layers as shown schematically in **Fig. 2**. Photon absorption

J_{sc} ,
 V_{oc} ,
FF

SI

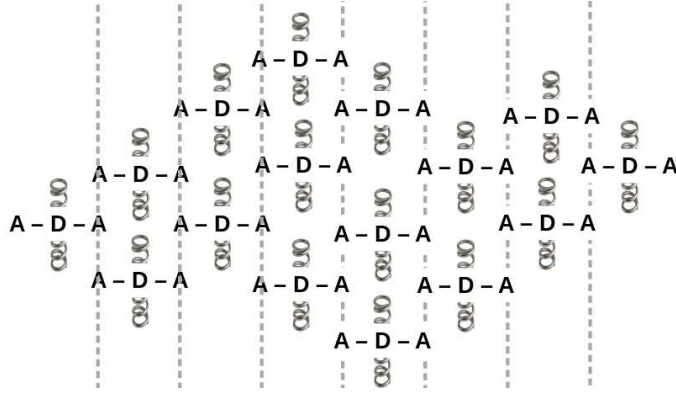


Figure 2: Schematic of the stacking of A-D-A molecules²⁸. Bulky out-of-plane side groups on the D units are represented by springs. The π -stacking of A units is emphasized by joining stacked A units with grey dotted lines.

and exciton formation may occur in the D unit which then leads to charge separation with D positively charged and A negatively charged. Charge recombination is minimized by stacking of A units in the crystal whose crystal structure allows the negative charges to conduct quickly away from the heterojunction. Unfortunately too much local crystallinity can also be harmful, so that bulky out-of-plane side groups (shown as springs in the figure) are used to control the stacking density. As we will show, and provided we neglect any absorption features at the DON:ACC heterojunction itself, photons are being absorbed and excitons are now being formed in both the DON and the ACC components, necessitating changes in the simple Scharber model for predicting OSC PCEs. In line with the philosophy underlying Scharber’s approach, we have presented a new finite-width approach with only one additional assumption beyond Scharber’s approach. Our description of the A-D-A ACC would seem to indicate that the stronger the acceptor A, the better the OSC should work. We will argue that the opposite occurs in the present case.

The rest of the paper is organized as follows. Computational details are given in the next section. Results are presented in Sec. 3, which is divided into three subsections. Our choice of methodology is carefully examined in the first subsection by comparing calculated results with experimental results from the literature. The next subsection focuses on calculations characterizing the relative acceptor strength of the A units and the consequences on physical properties. The third and final subsection predicts CV FMO

values, absorption spectra, discusses the degree of charge separation in the charge transfer excitations, and applies our finite-width theory to predict OSC PCEs for our candidate molecules. Section 4 gives our concluding discussion.

2 Computational Details

The five molecules shown in Fig. 1 have been replaced by somewhat simpler model compounds by replacing the four very flexible *n*-hexyl (i.e., C₆H₁₃) chains in the molecules with methyl groups. The resultant molecules are much less flexible, making their geometries easier to optimize. The validity of this approximation will be tested in Sec. 3 and found to be acceptable.

Unless otherwise stated, all calculations were carried out using the GAUSSIAN 09 program package²⁹. Following the terminology of the Pople school, the triplet functional/basis set/solvent defines our theoretical model chemistry (TMC). Geometries were optimized in chloroform using the integral equation formalism (IEF) variant of the implicit solvent polarizable continuum model (PCM) (see Ref.³⁰ for a review of PCM models) using DFT functional³¹ with the 6-311G(d,p) basis set³²⁻³⁴. After testing three hybrid functions (B3LYP³⁵, PBE0³⁶, B3PW91³⁷) and a range-separated hybrid functional (HSEH1PBE)³¹ for the geometry optimization of \mathbf{M}_0 , it was decided to use HSEH1PBE for all of the molecules.

TMC

IEF,
PCM

Start geometries for the optimizations were constructed using the GAUSS VIEW program³⁸. MOLDEN³⁹ was also used for visualizing molecules. Vibrational frequencies were calculated to verify that the optimized geometries are true minima. Optimized geometries and the lowest vibrational energies are given in the SI. Translational and rotational energies often come out as imaginary but of small magnitude (less than 11.0 cm⁻¹) because of numerical approximations.

Once their geometries were optimized, these same model molecules were used to calculate all of the properties reported here. Note that we will show that the replacement of the four *n*-hexyl alkyl groups by simpler methyl groups has little direct effect on the electronic properties of these molecules. However the large flexible side groups (X) do increase solubility and help to control local aggregation in the solid state. Such local aggregation is important because it may help to facilitate the transformation of a charge

X

transfer state at the DON:ACC interface into fully separated charges, but may also have a negative effect on OSC flexibility and morphology. In particular, a very similar molecule with *p*-hexylphenyl groups rather than *n*-hexyl groups is known to have a crystal structure typical of ideal J-aggregation²⁸, meaning that absorption spectra are expected to be red shifted and to show additional peaks due to intermolecular stacking interactions (see, e.g., Ref.⁴⁰ for a brief history and review of excitonic effects on spectra).

CV redox potentials were also calculated in acetonitrile as this is closer to the preferred solvent used in the experimental measurements. Outside of the field of materials for electronics applications, CV data is simply described as measuring oxidation and reduction potentials. However, within the field of materials for electronics applications, these redox potentials are usually reported as frontier molecular orbital (FMO) energies. [An exception is a University-level general chemistry textbook that also discusses materials for electronics applications (see page 779 of Ref.⁴¹).] The identification of CV redox potentials as FMO energies is misleading⁴², causing some researchers to misidentify DFT HOMO and LUMO energies with CV HOMO and CV LUMO energies. Proper calculation of CV FMO energies involves calculating the Gibbs' free energy for ionization and electron attachment in solution⁴³. However it is a reasonable approximation to ignore entropic and pressure volume effects and just calculate ionization potentials (IPs) and electron affinities (EAs) in solution. As we shall see, we do obtain CV FMO energies with this method which agree reasonably well with experiment. IP, EA

Sometimes though, we would like to compare experimental CV FMO energies directly with DFT FMO energies, but is this really reasonable? The answer is that we *can* use the DFT FMO energies as approximate CV FMO energies *provided* we are very careful about how we do this. The reason goes back to the basics of Kohn-Sham DFT⁴⁴ itself. For reasons of simplicity and rigor we will specialize to the HOMO energy. In the original theory, the exchange-correlation potential v_{xc} was a purely multiplicative function for which the HOMO energy would be minus the ionization potential ($E_{\text{HOMO}} = -\text{IP}$), provided v_{xc} is exact. (see, e.g., Ref.⁴⁵ and references therein). However it was later discovered that the exact v_{xc} contains a particle-number derivative discontinuity^{46,47} which is absent in both the local density approximation (LDA) and in generalized gradient approximation (GGA) functionals, leading to the HOMO energy to be closer to minus the average of the ionization potential and the electron affinity ($E_{\text{HOMO}} = -(\text{IP} + \text{EA})/2$) LDA, GGA

within a reasonable parabolic approximation. This behavior is in marked contrast to the familiar Koopmans’ interpretation of Hartree-Fock molecular orbital energies that $E_{\text{HOMO}} \approx -\text{IP}$ and $E_{\text{LUMO}} \approx -\text{EA}$ ⁴⁸. It also means that the introduction of global and range-separated functionals with part exact exchange is no longer Kohn-Sham DFT, even if the total energies are (to within a localization of v_{xc}) DFT energies. In particular, varying the functional, and particularly how the exact exchange enters the functional, provides a way to *tune* the orbital energies. In fact, the concept of optimal tuning was introduced in TD range-separated hybrid DFT as a way to fix the range-separation parameter while simultaneously improving charge-transfer excitation energies⁴⁹. In so far as DFT orbital energies are much more sensitive to the choice of functional than are DFT total energies, tuning the functional can allow the DFT FMO energies to approach CV FMO energies calculated using the DFT ΔSCF procedure with the same functional. In a somewhat similar spirit, and knowing that DFT orbital energies and ΔSCF energies have been frequently noted to be linearly correlated (see, e.g., Refs.^{50–52}), we have tried several different functionals to see which, if any of them, give DFT FMO energies closest to experimentally obtained CV FMO energies. (See Sec. 3.)

TD-DFT absorption spectra were calculated in chloroform using the same HSEH1PBE/6-311G(d,p) level of calculation. The absorption spectra have been calculated for 30 singlet-singlet transitions and were gaussian-convoluted before comparing with experimental spectra. The SWIZARD program⁵³ was used to help assign the calculated transitions.

DON:ACC PCEs were estimated using a simple home-made PYTHON program for making Scharber plots designed to vary DON at constant ACC (see the SI) which was modified as further described in Sec. 3 to be able to vary ACC at constant DON.

Charge transfer within our A-D-A ACC molecules was analyzed using transition density matrix (TDM) heatmaps made using version 3.1 of the MULTIWFN program^{54,55}. This is also further described in Sec. 3.

TDM

3 Results

Our results are divided into three parts: (1) validation of our choice of TMC—namely, the HSEH1PBE/6-311G(d,p) with the PCM implicit solvent model for chloroform—by

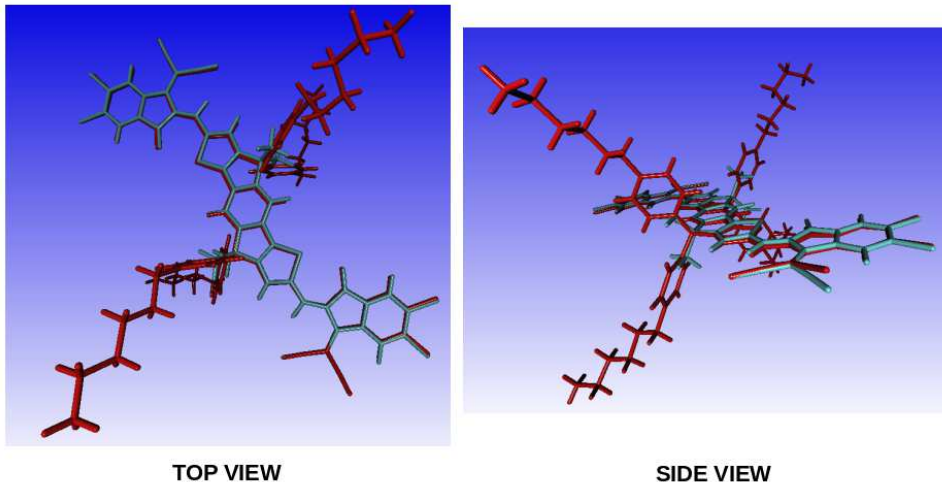


Figure 3: Comparison of the single-crystal X-ray geometry of IDIC(tris(4-hexylphenyl))-4Cl (Cambridge Crystallographic Data Centre database identifier YISJOC, deposition number 1860549, Ref.²⁸) in red with our HSEH1PBE/6-311G(d,p)/PCM(chloroform) optimized geometry for IDIC(tetramethyl)-4Cl in green.

comparison against experimental values for IDIC-4Cl; (2) use of various analytical tools to characterize chemical notions such as relative donor/acceptor abilities and chemical reactivity for our four candidate molecules; and finally (3) concrete physical predictions regarding the physical properties of the candidate molecules.

3.1 Theoretical Model Chemistry Validation

We first validate our TMC against reported experimental results for IDIC-4Cl. A caveat is that there are several different IDIC-4Cl molecules reported in the literature (see the SI), albeit with similar electronic properties. Our simplified model [IDIC(tetramethyl)-4Cl] is expected to be able to reproduce the properties of all of these different IDIC-4Cl molecules, to the extent that results are independent of the side chains (X).

We were able to find a single-crystal X-ray geometry for IDIC-4Cl, but only for IDIC(tris(4-hexylphenyl))-4Cl²⁸. **Figure 3** shows a superposition of this structure with our HSEH1PBE/6-311G(d,p)/PCM(chloroform) optimized geometry for IDIC(tetramethyl)-4Cl using MOLDEN³⁹. Except for the side chains, the structures are remarkably well matched. The (x, y, z) -coordinates of HSEH1PBE/6-311G(d,p)/PCM(chloroform) opti-

X	CV HOMO Energy	CV LUMO Energy	CV H-L Gap	Reference
IDIC(X)				
tetrakis(4-hexylphenyl)	-5.70 eV	-3.87 eV	1.83 eV	28
tetraoctyl	-5.77 eV	-3.98 eV	1.78 eV	56
tetrahexyl	-5.69 eV	-3.91 eV	1.78 eV	57
IDIC(X)-4Cl				
tetrakis(4-hexylphenyl)	-5.78 eV	-4.02 eV	1.76 eV	28
tetraoctyl	-5.88 eV	-3.98 eV	1.90 eV	58,59
tetraoctyl	-5.85 eV	-4.05 eV	1.80 eV	56
tetrahexyl	-5.81 eV	-4.01 eV	1.80 eV	60
tetramethyl	-5.99 eV	-3.89 eV	2.10 eV	Δ SCF
tetramethyl	-4.81 eV	-4.04 eV	1.77 eV	“Koopmans”

Table 1: Comparison of experimental and calculated (PW) CV FMO values. The experimental CV FMO energies are typically measured in acetonitrile with $(n\text{-Bu})_4\text{NPF}_6$ (0.1 M) as supporting electrolyte, Pt wire as counter electrode, and Ag/Ag⁺ as reference electrode. Our calculations are for the HSEH1PBE/6-311G(d,p)/PCM(chloroform) theoretical model chemistry.

mized IDIC(tetramethyl)-4Cl geometry are given in the SI.

CV data are routinely reported for molecules which are important for organic electronics. CV FMO energies are obtained by measuring the redox potentials for the molecule in question and for ferrocene under the same conditions, correcting the redox potential of the molecule using ferrocene redox potential, and then adding an additional correction to put the CV HOMO and CV LUMO on the absolute vacuum scale.

Table 1 shows measured CV FMO energies for several IDIC and IDIC-4Cl molecules taken from the literature. IDIC(tetrahexyl) and IDIC(tetraoctyl) have nearly identical CV FMO energies. Similarly IDIC(tetrahexyl)-4Cl and IDIC(tetraoctyl)-4Cl have nearly identical CV FMO energies, consistent with the idea that the hexyl and octyl groups are chemically similar, neither donating nor accepting electrons. This comforts us in our expectation that IDIC(tetramethyl)-4Cl should also have very similar CV FMO energies.

Interestingly, as the CV HOMO and CV LUMO energies of IDIC(tetrakis(4-hexylphenyl))

	B3LYP ^a	PBE0 ^b	B3PW91 ^c	HSEH1PBE ^d	Expt. ^e
LUMO	-3.79	-4.25	-3.87	-4.04	-4.01
HOMO	-5.93	-5.47	-6.04	-5.81	-5.81
$E_{\text{H-L}}$	2.14	1.22	2.17	1.77	1.79

Table 2: The energy levels of HOMO (eV), LUMO (eV), and the energy gap $E_{\text{H-L}}$ (eV) for the acceptors molecule obtained by DFT/6-311G(d,p) in chloroform solution. ^a Ref. ³⁵. ^b Ref. ³⁶. ^c Ref. ⁶¹. ^d Ref. ³¹. ^e CV FMO energies for IDIC(tetrahexyl)-4Cl from Ref. ⁶⁰.

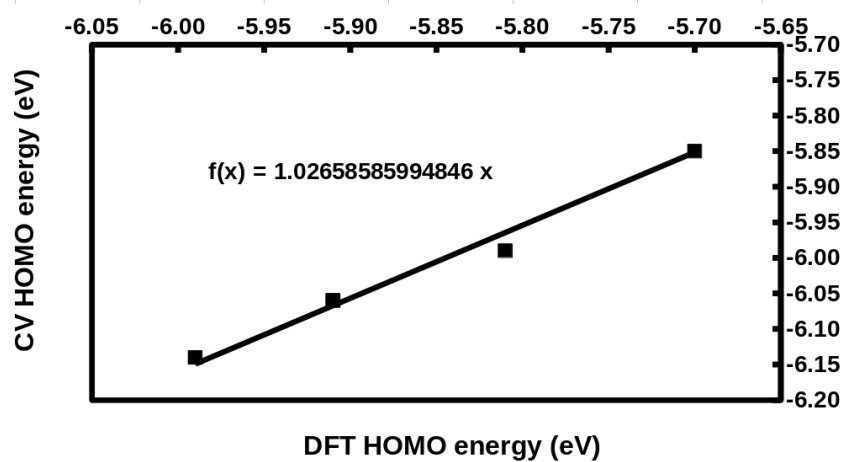
are greater than those of IDIC(tetraoctyl), the 4-hexylphenyl should also be a (+M) electron donor. However, the experimental CV HOMO and CV LUMO energies of IDIC(tetrahexyl) are very similar to those of IDIC(tetrakis(4-hexylphenyl)). This may simply be a question of differences in how the CV FMO energies were measured and how accurately they could be determined experimentally since the CV HOMO energy of IDIC(tetrakis(4-hexylphenyl))-4Cl is higher than that of IDIC(tetrahexyl)-4Cl and of IDIC(tetraoctyl)-4Cl. Thus the classification of 4-hexylphenyl as a +M donor seems reasonable. Note that the experimental CV LUMO energies are all very similar for the three IDIC-4Cl molecules.

Calculated ΔSCF CV FMO energies are shown in Table 1. In Sec. 2, we raised the question of which functionals give DFT FMO energies closest to the experimental CV FMO energies? **Table 2** shows that¹, of the functionals tested, the HSEH1PBE functional meets this criterion best. In the end, because of the fit to experiment, we think that our DFT FMO energies might even be a better predictor of experimental CV FMO energies, although we prefer to report CV FMO energies calculated using the ΔSCF procedure.

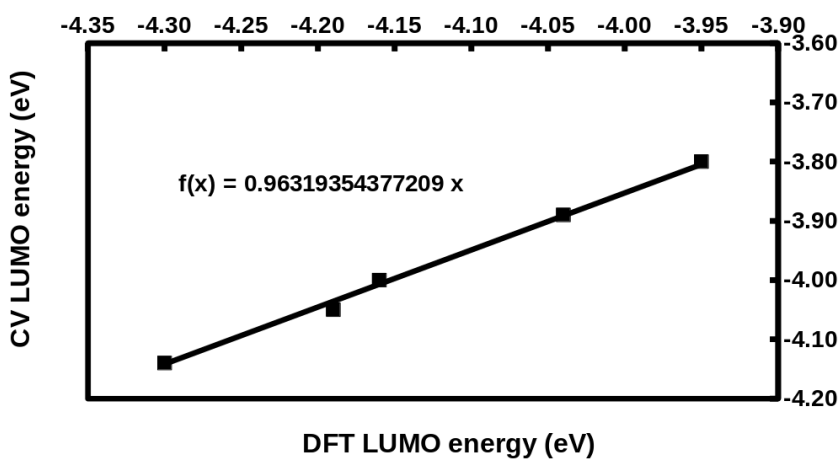
Absorption spectra are another type of data which are routinely reported for molecules which are important for organic electronics. Care must be taken in measuring solution spectra because flat polyaromatic molecules, such as substituted IDICs are likely to form

¹Note that B3LYP here is the original GAUSSIAN B3LYP functional, rather than the “corrected” B3LYP functional which is the default in the TURBOMOL and ORCA programs and which gives very different total energies. The latter B3LYP functionals from the original GAUSSIAN version by replacing GAUSSIAN’s VWN RPA LDA parameterization with the original VWN Monte Carlo LDA parameterization of Vilko, Wilk, and Nusair⁶² (called VWN5) in GAUSSIAN.

(a)



(b)



(c)

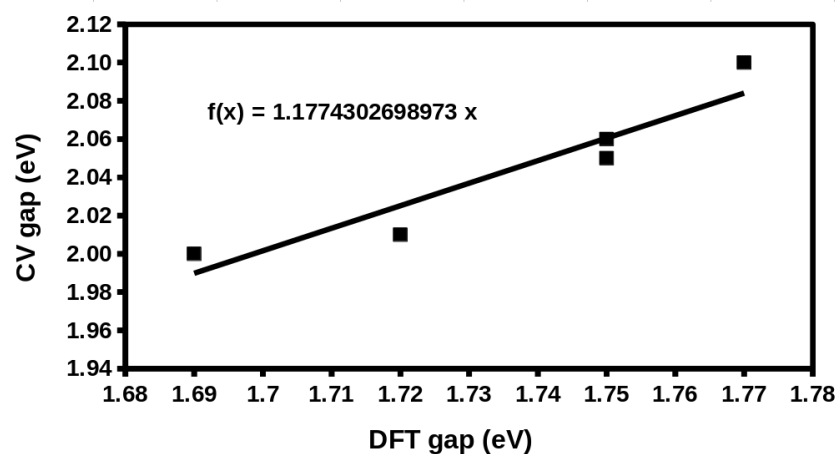


Figure 4: Forced intercept least squares fit between DFT FMO energies and CV (Δ SCF) FMO energies calculated using the HSEH1PBE/6-311G(d,p)/PCM(chloroform) theoretical model chemistry.

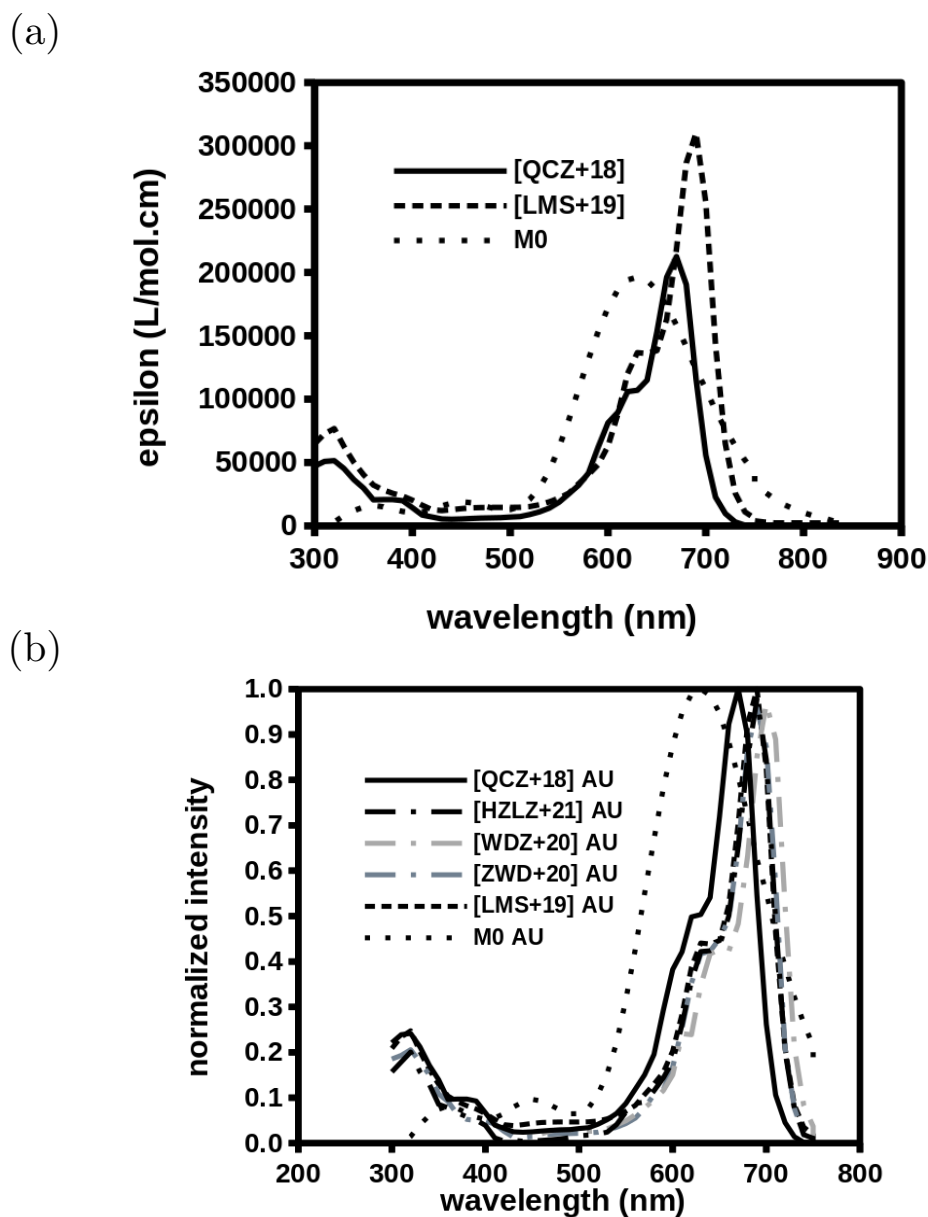


Figure 5: Absolute (a) and renormalized (b) IDIC(X)-4Cl absorption spectra from the literature and calculated using TD-DFT within the HSEH1PBE/6-311G(d,p)/PCM(chloroform) theoretical model chemistry: [QCZ+18], X = tetrakis(4-hexylphenyl), in chloroform²⁸; [WDZ+20], [ZWD+20], [HZZ+21], X = tetraoctyl, in chloroform^{56,58,59}; [LMS+19], X = tetrahexyl, in chloroform⁶⁰; and M_0 , X = tetramethyl, present calculations.

red-shifted J-aggregates²⁸. We will come back to this below. In general IDIC-Cl spectra are found to be red shifted with respect to the corresponding IDIC spectra^{28,56}, consistent with the previous observation that chloro groups tend to close the CV HOMO-LUMO gap. **Figure 5** shows literature spectra for IDIC(X)-4Cl molecules digitized using the interactive internet-based WEBPLOTDIGITIZER⁶³ and combined into a single diagram. It is immediately clear from the figure that there is no significant difference between IDIC(tetrahexyl)-4Cl and IDIC(tetraoctyl)-4Cl which suggests that we are justified in using our IDIC(tetramethyl)-4Cl model. However the IDIC(tetrakis(4-hexylphenyl))-4Cl spectrum is blue shifted with respect to the other IDIC-4Cl spectra. This suggests an opening of the IDIC-4Cl CV HOMO-LUMO gap in the case of IDIC(tetrakis(4-hexylphenyl))-4Cl. It may also be that some aggregate formation was occurring in the solutions for which the other IDIC-4Cl spectra were measured.

Our calculated TD-DFT spectrum is also shown in Fig. 5. Following usual practice, the calculated spectrum has been gaussian-convoluted. In this case, the full-width at half maximum (FWHM) of the gaussian that was used is a bit too broad compared with the measured peak widths. This is probably also why no shoulder is observed in the theoretical spectrum while a short wavelength shoulder is quite evident on the main peak in the experimental spectrum. More importantly the maximum of the main peak in the TD-DFT calculation is red shifted compared to the experimental IDIC(tetrahexyl)-4Cl peak by about 0.2 eV, which is within the expected limit of the computational method.

FWHM

A third type of data reported in this field is the very *raison d'être* for the field. These are the performance parameters of actual organic photovoltaic cells determined from current density J versus voltage V curves. Such curves have the general form predicted by some variant of the Shockley diode equation^{64,65},

$$J = J_0 \left[1 - \exp \left(\frac{V + IR}{nV_T} \right) \right] + J_{ph}, \quad (1)$$

where $V_T = k_B T / e$ and J_{ph} is the photocurrent. Rather than try to invert the equation to obtain J_0 , R , and the ideality factor n , it is traditional to report another set of parameters to characterize photovoltaic cell performance. These are the V_{oc} , J_{sc} , and FF. V_{oc} is related to the difference between the difference between the CV LUMO energy of the acceptor and the CV HOMO energy of the donor which provides the driving force for charge separation at the donor-acceptor interface. Empirically, for some solar cells, with ohmic contacts, it

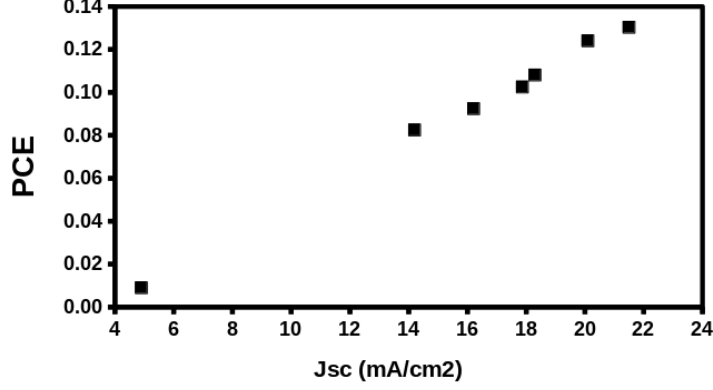


Figure 6: Graph of the data from Table 3 showing the near proportionality of the photoconversion efficiency and the open-circuit current.

has been found that,

$$eV_{oc} = E_{CV\ LUMO}^{ACC} - E_{CV\ HOMO}^{DON} - \delta. \quad (2)$$

The δ correction likely arises for several physical reasons. It is already found in the Shockley diode equation itself^{15,16}. However additional contributions may arise due to band bending in the electrodes⁶⁶ or from the simple fact that the values of the CV FMO energies used in the equation are obtained under different conditions than those in actual solar cells. J_{sc} is related to how much light is converted into electrical energy, and so it is ultimately also related to the absorption spectrum. The FF measures how close the J-V curve is to a perfect rectangle. Physically the FF is a monotonically increasing function of V_{oc}/nV_T ⁶⁷. High values of FF are favored by large open-circuit voltages and low values of the ideality factor n . The value of the ideality factor is closely related to morphology as low values of n mean that charges travel farther before electron-hole recombination occurs. Together, these allow the calculation of the PCE η via the equation,

$$\eta = \frac{J_{sc}V_{oc}FF}{P_s}, \quad (3)$$

where P_s is the solar power. Under AM 1.5G conditions,

$$P_s = \int_0^{\infty} F(\lambda) d\lambda = 99.971 \text{ mW/cm}^2, \quad (4)$$

where $F(\lambda)$ is the irradiance (in $\text{W/m}^2.\text{nm}$).

Table 3 shows actual experimental data taken from the literature. **Figure 6** shows that, for this data, the PCE is nearly proportional to J_{sc} . This is because both the FF and

CV HOMO Energy	CV LUMO Energy	V_{oc}	J_{sc}	FF	PCE
PBDB-T2Cl:IDIC(tetrakis(4-hexylphenyl))-4Cl ²⁸					
-5.51 eV	-3.57 eV	0.83 V	16.21 mA/cm ²	68.69%	9.24%
BSCl:IDIC(tetraoctyl)-4Cl ⁵⁹					
-5.55 eV	-3.30 eV	0.865 V	21.5 mA/cm ²	70.0%	13.03%
BSCl-C1:IDIC(tetraoctyl)-4Cl ⁵⁸					
-5.59 eV	-3.34 eV	0.564 V	4.9 mA/cm ²	33.9%	0.90%
BSCl-C2:IDIC(tetraoctyl)-4Cl ⁵⁸					
-5.58 eV	-3.39 eV	0.865 V	20.1 mA/cm ²	71.3%	12.40%
BSCl-C3:IDIC(tetraoctyl)-4Cl ⁵⁸					
-5.55 eV	-3.37 eV	0.870 V	14.2 mA/cm ²	67.0%	8.25%
ZR1-Cl:IDIC(tetraoctyl)-4Cl ⁵⁶					
-5.51 eV	-3.60 eV	0.87 V	18.30 mA/cm ²	68.03%	10.81%
PM6:IDIC(tetrahexyl)-4Cl ⁶⁰					
-5.50 eV	-3.61 eV	0.767 V	17.87 mA/cm ²	74.76%	10.25%

Table 3: Photovoltaic properties for some donor:IDIC(X)-4Cl solar cells. The CV FMO energies are for the donor. The reader is referred to the original articles for an explanation of the donor molecule name.

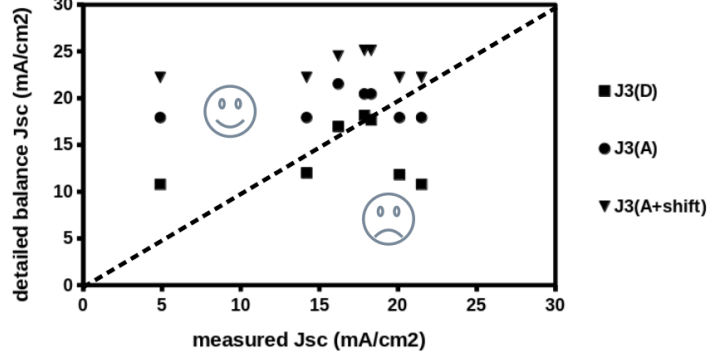


Figure 7: Detailed balance short-circuit currents calculated from the acceptor CV gap with and without red shift and from the donor CV gap. In this diagram A stands for ACC and D stands for DON.

V_{oc} are essentially the same for all of the photocells. Except for the somewhat aberrant BSCl-Cl:IDIC(tetraoctyl)-4Cl photocell, the value of the FF varies from 67.0% to 74.76% with an average value of 69.96%. The values of V_{oc} are too similar to confirm an equation of the form of Eq. (2). Instead, we assume the form of the equation and calculate that the average value of $\delta = 0.74$ eV.

But how can we estimate the short-circuit current? The external quantum efficiency $\text{EQE}(\lambda)$ is the percent of photons converted into current. It can be shown that,

$$J_{sc} = \int_0^{\infty} \text{EQE}(\lambda) F(\lambda) \lambda d\lambda. \quad (5)$$

EQE

Shockley and Queisser introduced the detailed balance (db) model which assumes that every photon whose energy exceeds the CV gap is absorbed and forms an electron-hole pair⁶⁸. Then

db

$$\text{EQE}(\lambda) = \theta(\lambda_g - \lambda), \quad (6)$$

where θ is the Heaviside (step) function, so that

$$J_{db}(E_g) = \int_0^{\lambda_g} F(\lambda) \lambda d\lambda, \quad (7)$$

where $\lambda_g = hc/E_g$ is the wavelength corresponding to the CV gap. An adequate approximation⁶⁹ to the experimental AM 1.5G irradiance⁷⁰ is given in Ref.⁶⁹ and leads to,

AM

$$J_{db}(E_g) = (73.531 \text{ mA/cm}^2) e^{-(0.440)(E_g/\text{eV})^{1.8617}}. \quad (8)$$

1.5G

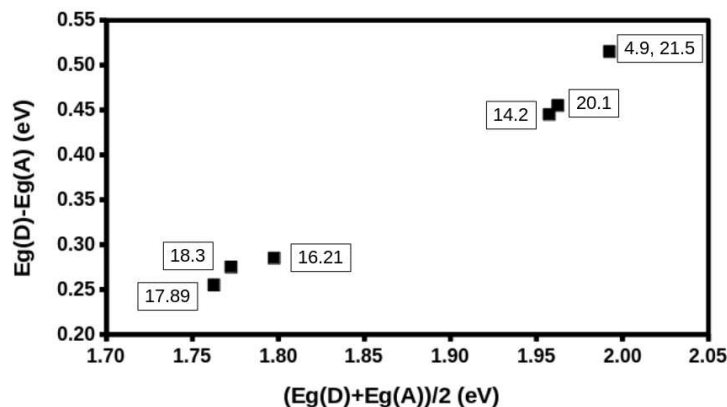


Figure 8: Gap difference versus average gap. The framed numbers are measured short-circuit currents in mA/cm². Note that the acceptor CV gaps include the red shift correction.

This allows us to obtain an upper limit on the PCE of the solar cells whose parameters are given in Table 3. Unlike organic solar cells with fullerene acceptors, it is no longer a good assumption that absorption and exciton formation takes place only in the DON. We must also test Eq. (8) for the ACC. (Note that we are ignoring absorption by heterojunction surface states, which seems a reasonable first approximation.) The detailed balance J_{sc} calculated for the acceptor and for the donor are compared with the measured J_{sc} in **Fig. 7**. Anything below the dashed line (frowny face region) represents a violation of energy conservation. This occurs both for the donor and for the acceptor, though it is worse for the donor. However it must be kept in mind that there is a significant red shift in the absorption spectrum in going from solution to the solid state (see SI-Spectral Shift). Subtracting this shift from the ACC CV gap restores energy conservation (smiley face region), indicating the importance of this small shift. The shifted acceptor point which is closest to the dashed line is the BSCl:IDIC(tetraoctyl)-4Cl solar cell whose 13.03% PCE is essentially the same as the detailed balance limit for this type of solar cell.

In previous work, Scharber constructed a contour plot of DON:PCBM bulk heterojunction solar cell PCEs as a function of the DON CV LUMO energy and the donor CV gap^{15,16}. It is an attempt to make an educated guess as to the best obtainable PCE for different DON polymers. This is, of course, tricky because it refers not to every solar cell, but only to the ones with optimal ohmic contacts, good morphology, etc. Scharber's

theory is very similar to what we have been doing here, except that Scharber assumed that all excitons are formed in the DON, which is reasonable for DON:PCBM solar cells. Here we see that excitons must also be formed in the ACC, hence necessitating a change in Scharber’s theory. Like Scharber, we will search for a description of the best J_{sc} consistent with the known DON and ACC band gaps. **Figure 8** shows that the difference between the DON and ACC CV gaps is nicely correlated with the average of the DON and ACC CV gaps. That is because the ACC CV gap is relatively constant compared to the DON CV gap. More importantly, we see that there is a general tendency for J_{sc} to increase as the band gap difference increases, *provided* we ignore the lower-performing solar cells with J_{sc} equal to 4.9 mA/cm² and to 14.2 mA/cm². This is justifiable because accurate benchmarking of organic solar cell performance requires a rigor which is often lacking in exploratory results reported in the literature. Certified performance numbers require very carefully prepared standard cells and must be performed by an independent third-party laboratory. Moreover, to quote Ref.⁴, “It is important to note that not all independent measurements performed by third-party laboratories are accepted for entry into the Solar Cell Efficiency Tables, as only nine laboratories are officially recognized.” Most of the time, this means that the performance data reported in the literature is not quantitatively reproducible and is often on the low side. Hence we feel justified in ignoring the solar cell with J_{sc} equal to 4.9 mA/cm². Ignoring the solar cell with J_{sc} equal to 14.2 mA/cm² is more debatable, but we feel that this experimental value is probably also underestimated. Of course, we could also have ignored the solar cells with J_{sc} equal to 16.21 mA/cm², 17.89 mA/cm², and 16.21 mA/cm², but we have chosen not to do so. Our theory here is that better performance is obtained by having absorption occurring at different wavelengths in the ACC and in the DON.

Let us be more precise. If absorption is included in the EQE, then the function becomes⁶⁹

$$\text{EQE}(\lambda) = 1 - e^{-\alpha(\lambda)\ell} = 1 - e^{-\beta\bar{\epsilon}(\lambda)}. \quad (9)$$

Here $\alpha(\lambda)$ is the attenuation coefficient in the Bouguer-Lambert law and ℓ is the path length. For a dilute solution, we recover Beer’s law,

$$\alpha(\lambda) = \ln(10)\epsilon(\lambda)c. \quad (10)$$

As organic solar cells are *not* dilute, Beer’s law is only indicative and this is why the

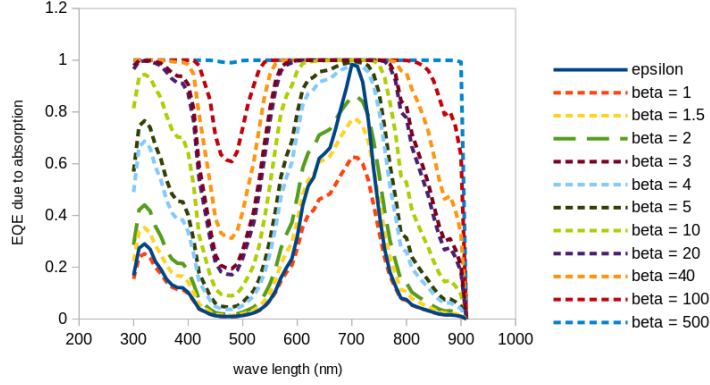


Figure 9: Graph of the function $\text{EQE}(\lambda) = 1 - \exp(-\beta\bar{\epsilon}(\lambda))$ for different values of β for IDIC-4Cl(tetrakis(4-hexylphenyl)).

absorption coefficient for organic solids is reported in terms of a normalized quantity,

$$\bar{\epsilon}(\lambda) = \frac{\epsilon(\lambda)}{\epsilon_{\max}} = \frac{\epsilon(\lambda)}{\epsilon_{\max}}. \quad (11)$$

Evidently for a dilute solution,

$$\beta = \ln(10)\epsilon_{\max}c\ell. \quad (12)$$

Figure 9 compares $\bar{\epsilon}(\lambda)$ with this $\text{EQE}(\lambda)$ for different values of β for the particular case of IDIC-4Cl(tetrakis(4-hexylphenol)). The CV gap is 1.76 eV which corresponds to a gap wave length of 705 nm which explains the position of the main peak in the absorption spectrum. The function $\text{EQE}(\lambda)$ is seen to be qualitatively similar to the absorption spectrum for $\beta \leq 2$. This is fine for very thin films. However as the path length increases for normal thicknesses, β increases and becomes more and more like a square function (case of $\beta = 500$). However, even for $\beta = 100$, we see a dip in $\text{EQE}(\lambda)$ near 450 nm. So much for the ACC.

Now consider the DON. It is expected to have an absorption peak at around the wave length corresponding to its CV gap. In the case of the highest performing solar cell, the donor is BSCl and its gap wave length is 551 nm which is expected to lead to an $\text{EQE}(\lambda)$ which will nicely fill in the dip in the ACC $\text{EQE}(\lambda)$ function. In contrast, the gap wave length of the PM6 solar cell is 656 nm whose $\text{EQE}(\lambda)$ is less likely to be able to fill in the dip in the ACC $\text{EQE}(\lambda)$ function. This explains the perhaps counter-intuitive result that increasing the donor gap may actually lead to an increased short-circuit current and a larger PCE rather than to a decreased short-circuit current and a smaller PCE.

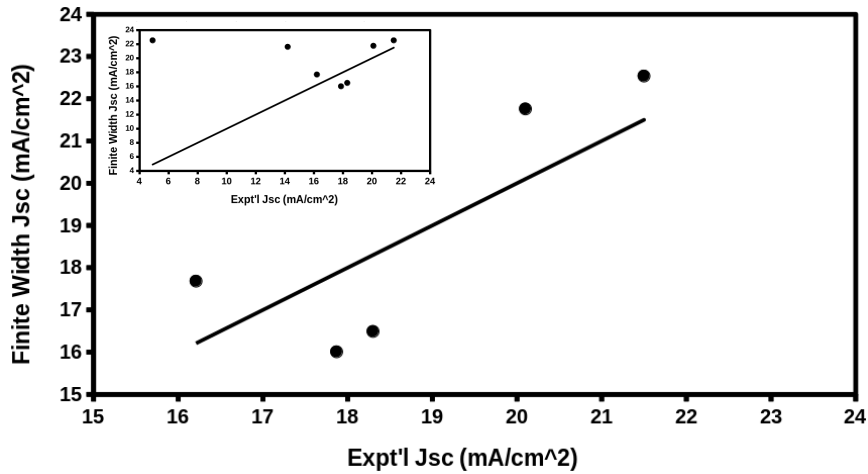


Figure 10: Comparison of fw model results with experimentally measured open-circuit currents using $\Delta\lambda = 200$ nm and DON CV FMO energies from Table 3 as well as a DON gap of of 1.78 eV for IDIC(tetrahexyl) and 1.80 eV for the other IDIC based upon data in Table 4. The inset shows the two data points that we have chosen to ignore on the grounds that they are likely underestimates of cell performance (see text). In both the main graph and the inset, the line represents perfect agreement between the model predictions and experimental measurements.

The Scharber plot is based upon detailed balance, which we have shown fails for the acceptor treated in this article. In order to make semi-quantitative educated guesses about how our candidate molecules might perform in real solar cells, we propose a simple model which we call the finite-width (fw) model. This model, while remaining computationally simple, tries to capture the fundamental physics that not every photon whose energy exceeds the band gap is going to be absorbed. To this end, we assume that both the ACC and the DON absorb photons in the wavelength range $(\lambda_g, \lambda_g + \Delta\lambda)$ where the gap wavelength λ_g differs for the ACC and the DON but we will insist on the same $\Delta\lambda$ cut-off for both the ACC and the DON. Then there are three different cases for any given photon wavelength: (i) it is neither within the absorption range of the DON nor of the ACC, (ii) it is within the absorption range of the DON or of the ACC but not both, or (iii) it is within the absorption range of both the DON and of the ACC and so has a 50/50 chance of being absorbed by each. We will also assume that $\lambda_g^{ACC} > \lambda_g^{DON}$. This leads to a fairly simple formula for the short-circuit current in our fw model,

$$J_{fw} = \frac{\min(\Delta\lambda, \lambda_g^{ACC} - \lambda_g^{DON}) + \Delta\lambda}{2} (\lambda_g^{DON} F(\lambda_g^{DON}) + \lambda_g^{ACC} F(\lambda_g^{ACC})) . \quad (13)$$

Figure 10 shows that this greatly overly simplified model works well for predicting J_{sc} . Hence we propose a modified Scharber model in which the db approximation is replaced by our fw approximation. Other parameters will be as above. This then provides a well-defined way to estimate solar cell performance via a modified Scharber plot based upon our fw model and using only data that we may calculate.

3.2 Comparison of Chemical Properties

Our ultimate interest is in predicting physical properties of importance for DON:ACC solar cells. The ACC molecules considered in this paper have the A-D-A form (see Fig. 1) first adapted as a strategy for making non-fullerene acceptors in 2015^{71,72}. In the previous subsection, we validated our TMC. The purpose of this subsection is to look at our candidate ACC molecules as a chemist might do.

The first thing that would like to consider are the optimized geometries shown in **Fig. 11**. They are essentially flat, with some minor curvature and/or twisting seen in the side view, but with methyl side groups sticking up out of the plane of the central D section. We do not study the effect of varying the side groups as they are mainly a

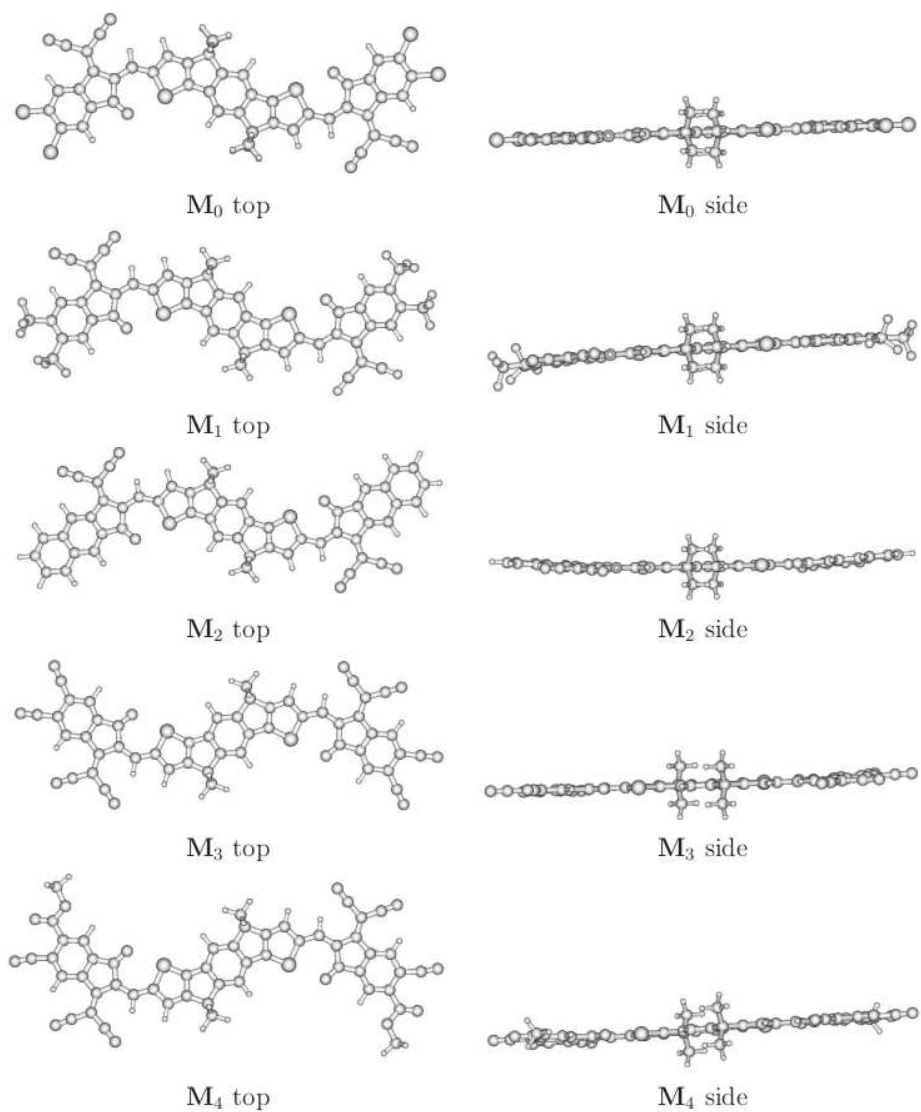


Figure 11: HSEH1PBE/6-311G(d,p)/PCM(chloroform) optimized geometries as visualized with MOLDEN³⁹.

way of controlling morphology. A crystal structure for an A-D-A ACC²⁸ shows that the side groups prevent π stacking of the D group. Instead the A groups π stack, forming a (presumably) conducting pile of aromatic rings. This is illustrated schematically in Fig. 2. Real organic solar cells are not crystalline but locally-crystalline aggregation is likely. Such locally-crystallinity has its pros and cons. On the one hand, the existence of crystal bands may help the charge-transfer (CT) state to evolve more quickly into fully charge-separated (CS) states by favoring band-like conductivity over hopping-like conductivity. Rapid charge separation also reduces the possibility for electron-hole recombination which is detrimental to solar cell efficiency. On the other hand, too much crystallinity may interfere with demixing of the ACC and DON, reducing the effective surface area of the ACC:DON heterojunction and possibly making the solar cell too mechanically rigid for some applications. This is why bulky side groups are typically added to be able to control the amount of aggregation so that it is neither too much nor too little.

CT, CS

The ACC molecules \mathbf{M}_0 , \mathbf{M}_1 , \mathbf{M}_2 , \mathbf{M}_3 , and \mathbf{M}_4 differ by modifications to the terminal A units in the A-D-A structure. Let us try to understand how these modifications affect the CV HOMO and CV LUMO energies, and the CV HOMO-LUMO gap in terms of chemical ideas. Many modern-day chemical concepts have only been given precise definitions relatively recently through the advent of conceptual DFT (CDFT, see Ref.⁷³ for a recent review), through the study of electron-number and density derivatives of molecular energies. In particular, CDFT helps to clarify the earlier ideas of FMO theory (see Refs.^{74,75}). It should probably be pointed out before going much further that chemical reactivity depends upon many factors. Reactions may be under steric control, charge control, or orbital control (as well as being affected by solvent effects). Pearson's well-known hard-soft acid-base (HSAB) theory concerns charge- versus orbital-control. For present purposes, it is useful to look at two density derivatives and their finite difference approximations. These are the chemical potential

CDFT

HSAB

$$\mu = \left(\frac{\partial E}{\partial N} \right)_v = \frac{E_{\text{CV HOMO}} + E_{\text{CV LUMO}}}{2} = -\chi, \quad (14)$$

which is just the negative of the Mullikan electronegativity ($\chi = -\mu$), and the hardness

$$\eta = \left(\frac{\partial^2 E}{\partial N^2} \right)_v = E_{\text{CV LUMO}} - E_{\text{CV HOMO}}. \quad (15)$$

Note that we have adopted the more modern definition of hardness which drops division by a factor of two. Note also that we have used the IP = $-E_{\text{CV HOMO}}$ and EA =

Compound	CV HOMO energy	CV LUMO energy	μ	η	ω
		Expt.			
IDIC(tetrahexyl) ⁵⁷	-5.69 eV	-3.91 eV	-4.80 eV	1.78 eV	6.47 eV
IDIC(tetrahexyl)-4Cl ⁶⁰	-5.81 eV	-4.01 eV	-4.91 eV	1.80 eV	6.70 eV
		Δ SCF			
M ₀	-5.77 eV	-3.97 eV	-4.87 eV	1.80 eV	6.59 eV
M ₁	-5.84 eV	-4.07 eV	-4.96 eV	1.77 eV	6.94 eV
M ₂	-5.70 eV	-3.93 eV	-4.82 eV	1.77 eV	6.55 eV
M ₃	-5.89 eV	-4.18 eV	-5.04 eV	1.71 eV	7.41 eV
M ₄	-5.84 eV	-4.10 eV	-4.97 eV	1.74 eV	7.10 eV
		“Koopmans”			
M ₀	-5.75 eV	-4.00 eV	-4.88 eV	1.75 eV	6.79 eV
M ₁	-5.82 eV	-4.10 eV	-4.96 eV	1.72 eV	7.15 eV
M ₂	-5.68 eV	-3.95 eV	-4.82 eV	1.73 eV	6.70 eV
M ₃	-5.87 eV	-4.21 eV	-5.04 eV	1.66 eV	7.65 eV
M ₄	-5.82 eV	-4.13 eV	-4.98 eV	1.69 eV	7.32 eV

Table 4: CV FMO energies and CDFT reactivity indices calculated at the HSEH1PBE/6-311G(d,p)/PCM(acetonitrile) level.

$-E_{CV\ LUMO}$ in our finite difference approximation which come from the Δ SCF calculations using the PCM implicit solvent model for molecules dissolved in acetonitrile. Interestingly our calculated CV HOMO-LUMO gap in acetonitrile is now closer to the experimentally-measured quantity in acetonitrile than was the case in Table 1 where calculations were carried out with chloroform as the solvent, thus further confirming our choice of TMC. Of particular importance for us is that these reactivity indices provide information about how energies change when the number of electrons change. In particular, placing the molecule in a constant chemical potential bath results in the spontaneous transfer of $-\mu/\eta$ electrons. This allows the electrophilicity index to be defined⁷⁶,

$$\omega = \frac{\mu^2}{2\eta}, \quad (16)$$

which is exactly the energy lowering due to charge transfer. Numbers are given for compounds in this paper in **Table 4**. *The columns marked $E_{CV\ HOMO}$ and $E_{CV\ LUMO}$ constitute predictions to be confirmed by cyclic voltammetry in acetonitrile.* The second part of the table (marked “Koopmans”) goes beyond the finite difference approximation and uses the FMO approximation to calculate the reactivity indices from directly DFT orbital energies. This second FMO approach is more approximate than the initial finite difference approach.

The electrophilicity index allows us to organize our analysis of key quantities as in **Fig. 12**. FMO theory predicts (see Fig.2 Supplementary information) that a good acceptor will lower the energies of both the HOMO and the LUMO, so that both should decrease as the electrophilicity index increases and this is indeed what is seen in Fig. 12. However the CV LUMO energy is much better linearly correlated with the electrophilicity index than is the CV HOMO energy, as might be expected given that the electrophilicity index is specifically designed to describe the stabilization resulting from donation of a pair of electrons into the LUMO. It is also apparent that the gap tends to decrease as the electrophilicity index increases, consistent with the appearance of the gap (η) in the denominator of the definition of the electrophilicity index [Eq. (16)]. However this is only a rough tendency and does not prevent \mathbf{M}_3 from having a smaller gap than \mathbf{M}_4 . The exact order of the acceptor strength depends upon how it is defined. If the definition is based upon the CV HOMO energy, then we have the following order of

$$\text{Acceptor Strength: } \mathbf{M}_3 > \mathbf{M}_4 \approx \mathbf{M}_1 > \mathbf{M}_0 > \mathbf{M}_2. \quad (17)$$

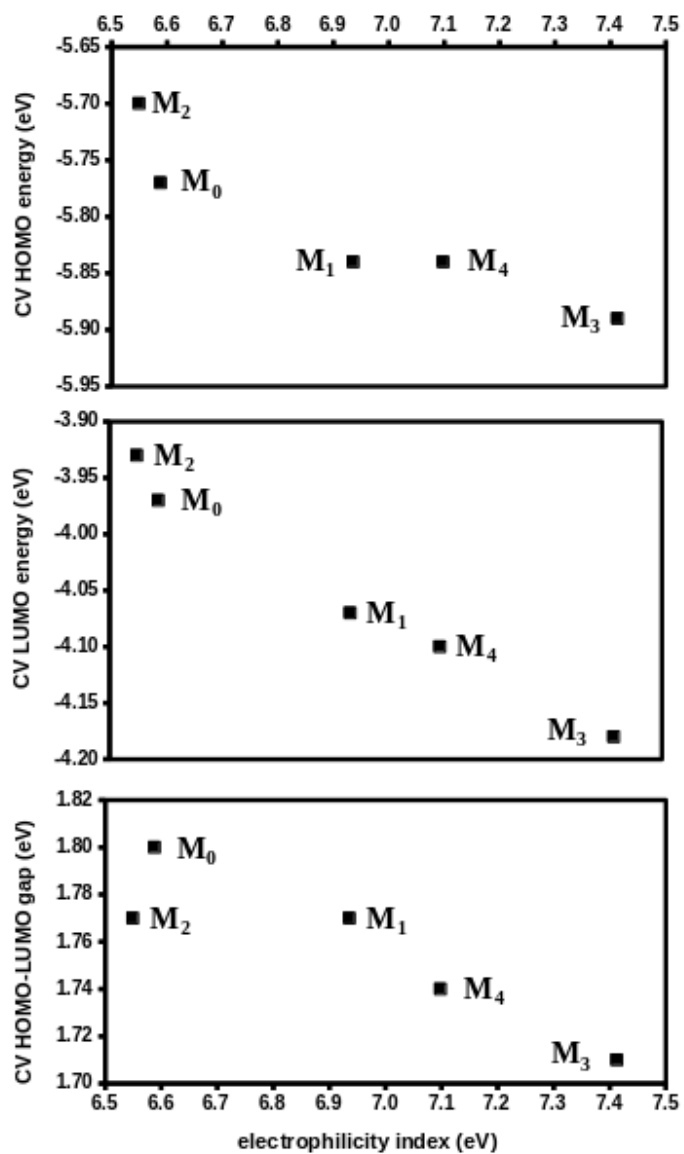


Figure 12: Correlation of CV FMO energies and the CV gap with the electrophilicity index calculated from the CV FMO energies.

Group	Hammett σ_m	Hammett σ_p	Remya & Suresh ΔV_C
CN	0.56	0.66	18.0
CF ₃	0.43	0.54	13.7
COOMe	0.37	0.45	8.2
Cl	0.37	0.23	7.0

Table 5: Some measures of the electron accepting capacity of chemical groups. The Hammett σ_m and σ_p values have been taken from the aqueous values in Table X of Ref.⁷⁷. The Remya & Suresh ΔV_C have been taken from Table 1 of Ref.⁷⁸.

However basing our definition on the electrophilicity index (or the CV LUMO energy) gives the more definite order of

$$\text{Acceptor Strength: } \mathbf{M}_3 > \mathbf{M}_4 > \mathbf{M}_1 > \mathbf{M}_0 > \mathbf{M}_2. \quad (18)$$

But does this make sense chemically? That is, \mathbf{M}_0 , \mathbf{M}_1 , \mathbf{M}_2 , \mathbf{M}_3 , and \mathbf{M}_4 differ by substitution of one functional group for another. Chemists can more easily recognize whether a functional group is electron donating or electron accepting than they can quantify that donating and accepting power. However the traditional way to do this in physical organic chemistry⁷⁹ is to use the Hammett σ which is the difference in the pK_a of benzoic acid and benzoic acid substituted in the *meta* or *para* positions. Some relevant Hammett σ_m and σ_p are tabulated in **Table 5**. The larger these σ , the stronger the electron acceptor. Remya and Suresh have recently developed another measure of donating and accepting power, but based upon differences of the molecular electrostatic potential at the nucleus of the carbon atom in the *para* position in substituted benzenes⁷⁸. Their values of ΔV_C is also tabulated in Table 5. If we assume that any of these values are additive, then we arrive at the following orders of accepting power for various combinations of accepting groups:

$$\begin{aligned}
 2\sigma_m(\text{CN}) = 1.12 &> \sigma_m(\text{CN}) + \sigma_m(\text{COOMe}) = 0.93 > 2\sigma_m(\text{CF}_3) = 0.86 > 2\sigma_m(\text{Cl}) = 0.74 \\
 2\sigma_p(\text{CN}) = 1.32 &> \sigma_p(\text{CN}) + \sigma_p(\text{COOMe}) = 1.11 \approx 2\sigma_p(\text{CF}_3) = 1.08 > 2\sigma_m(\text{Cl}) = 0.46 \\
 2\Delta V_C(\text{CN}) = 36.0 &> 2\Delta V_C(\text{CF}_3) = 27.4 \approx \Delta V_C(\text{CN}) + \Delta V_C(\text{COOMe}) = 26.2 > 2\Delta V_C(\text{Cl}) = 14.0.
 \end{aligned} \quad (19)$$

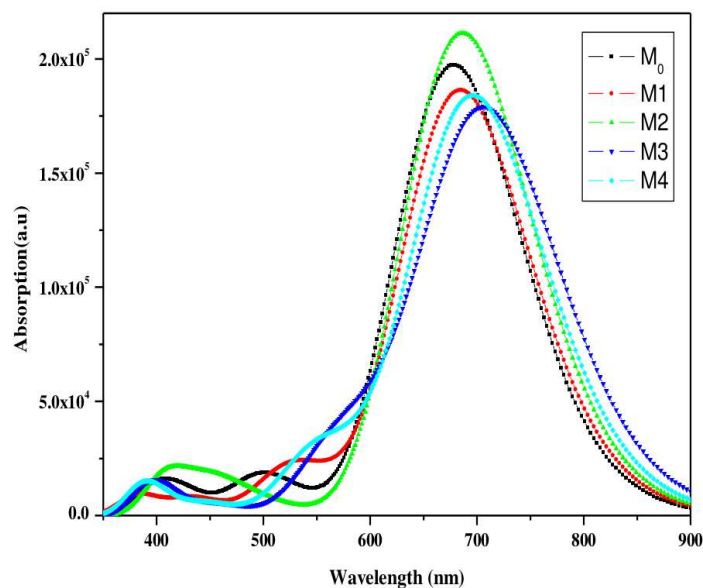


Figure 13: Absorption spectra calculated at the TD-HSEH1PBE/6-311G(d,p)/PCM(chloroform) level. Note that Epsilon (ϵ) is the molar extinction coefficient.

This tells us nothing about the end group used in making \mathbf{M}_2 but otherwise confirms Eq. (17) [Eq. (18) in the case of σ_m]. Hence our results are indeed consistent with those of traditional chemical theory.

3.3 Prediction of Physical Properties

We turn now to the prediction of physical properties for our candidate molecules. Of course, the CV FMO energies given in Table 4, and extensively discussed in terms of their chemical meaning, are already one prediction that may be confirmed by cyclic voltammetry in acetonitrile. Other important properties are the absorption spectrum in chloroform and predictions of solar cell performance.

Calculated absorption spectra are shown in **Fig. 13**. They are remarkably similar but there are small shifts in the position of the main peak (**Table 6**). The calculations show that the main peak is the singlet HOMO \rightarrow LUMO transition. As such, we might expect a good correlation between the energy of the main peak of the chloroform absorption spectrum with the CV gap in acetonitrile. This is exactly what is seen in **Fig. 14(a)** with the absorption maximum being almost exactly 0.04 eV higher than the CV HOMO-

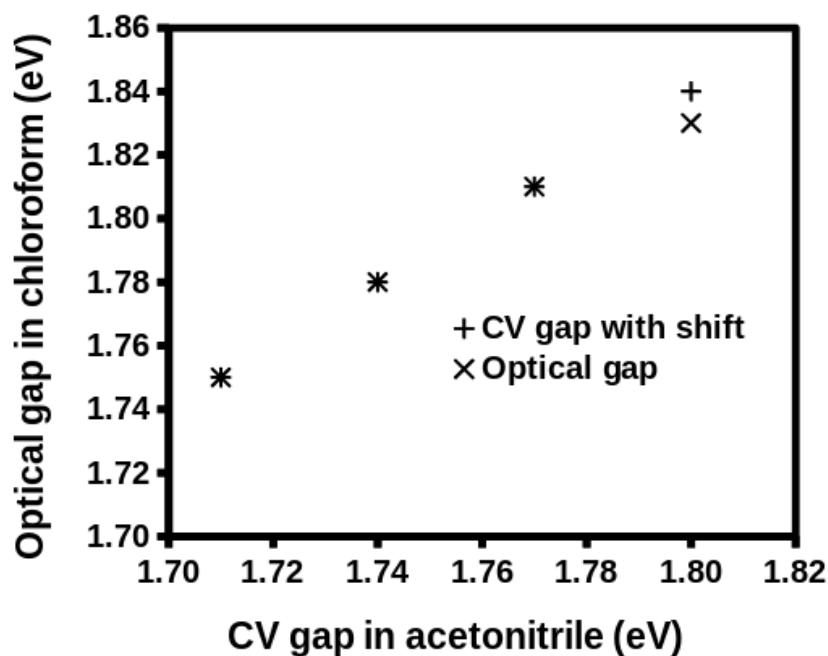
Molecules	λ_{\max}	E_{opt}	f	$R_{g,e}$
\mathbf{M}_0	678 nm	1.83 eV	2.73	4.13 Å
\mathbf{M}_1	684 nm	1.81 eV	2.57	4.03 Å
\mathbf{M}_2	686 nm	1.81 eV	2.92	4.29 Å
\mathbf{M}_3	708 nm	1.75 eV	2.44	3.99 Å
\mathbf{M}_4	696 nm	1.78 eV	2.53	4.03 Å

Table 6: Calculated absorption maxima ($\lambda_{\max} = E_{\text{opt}}/hc$, where “opt” stands for “optical”) and oscillator strengths (f) calculated at the TD-HSEH1PBE/6-311G(d,p)/PCM(chloroform) level. All transitions are essentially pure singlet HOMO \rightarrow LUMO. The quantity $R_{g,e}$ is a measure of charge separation distance as calculated from the transition dipole moment [see Eq. (24)].

Compounds	IP (eV)	EA (eV)	E_{fund} (eV)	E_{opt} (eV)	E_b (eV)
\mathbf{M}_0	-5.99	-3.89	2.10	1.82	0.28
\mathbf{M}_1	-6.06	-4.00	2.06	1.81	0.25
\mathbf{M}_2	-5.85	-3.80	2.05	1.81	0.24
\mathbf{M}_3	-6.14	-4.14	1.98	1.75	0.23
\mathbf{M}_4	-6.06	-4.05	2.01	1.78	0.23

Table 7: Calculation results of IP, EA, fundamental gap, first singlet excitation energies, and exciton binding energies of the reference and investigated acceptor molecules.

(a)



(b)

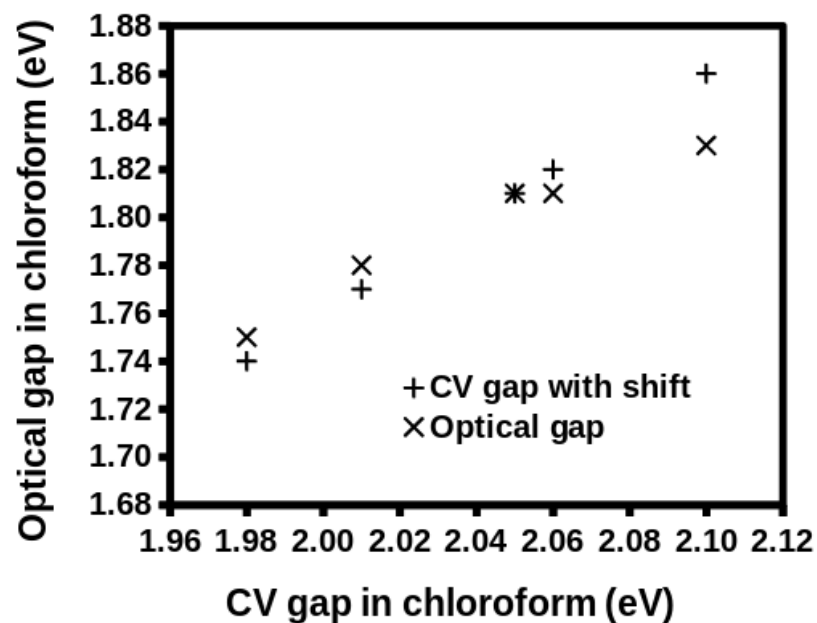


Figure 14: Correlation between the CV gap calculated in (a) acetonitrile and in (b) chloroform and the energy of the absorption maximum (optical gap) calculated in chloroform. When the CV gap is shifted down by an exciton binding energy of -0.04 eV (CV gap in acetonitrile) or 0.24 eV (CV gap in chloroform), then the shifted CV gap nearly coincides with the optical gap.

LUMO gap. Upon reflection, the near equivalence of the optical and CV HOMO-LUMO gaps is a little surprising as the shift has the wrong sign. The exciton binding energy E_b for a molecule \mathbf{M} is ΔE for the reaction,



E_b

In the Hartree-Fock two orbital two electron model (TOTEM) with frozen orbitals⁸⁰,

TOTEM

$$E_b = \text{CV LUMO} - \text{CV HOMO} - [LL|HH] + [HL|LH] , \quad (21)$$

where the HOMO-LUMO coulomb integral $[LL|HH] > 0$ is greater than the HOMO-LUMO exchange integral $[HL|LH] > 0$. Hence the exciton binding energy E_b is expected to be *larger* than the fundamental gap (CV LUMO – CV HOMO). In fact, it is *when the optical and fundamental gaps are calculated in the same solvent*. Table 7 shows the CV FMO energies recalculated in chloroform, instead of acetonitrile. This leads to the plot shown in Fig. 14(b) where it is seen that the exciton binding energy is indeed larger than the CV HOMO-LUMO gap. Comparing the optical gap calculated in chloroform with the CV HOMO-LUMO gap calculated in the more polar acetonitrile lead to a fortuitous, but misleading, coincidence of the two gaps, which has been corrected when the same solvent is used throughout.

Figure 15 shows the FMO isosurfaces for the the A-D-A molecules studied in this paper. It is qualitatively clear that HOMO density on D is being transferred to the LUMO density on A, making them charge-transfer excitations. Such excitations create electron-hole pairs whose dissociation leads to, but whose recombination prevents, charge transport. Characterizing these charge transfer excitations is not as obvious as might first be assumed because they may represent states that separate charge in equal but opposite directions so that, on average, no real transport of charge takes place⁴⁰. A way around this dilemma is to calculate and analyze the TDM

$$\gamma^{(0,I)}(1, 2) = \langle \Psi_0 | \hat{\psi}^\dagger(2) \hat{\psi}(1) | \Psi_I \rangle , \quad (22)$$

for each transition $0 \rightarrow I$ condensed to atoms

$$\Omega_{A,B} = \int_A d1 \int_B d2 |\gamma^{(0,I)}(1, 2)|^2 , \quad (23)$$

where the first integral is over the electron coordinates associated with atom A and the second integral is over the hole coordinates associated with atom B. The quantity $\hat{\psi}(i)$

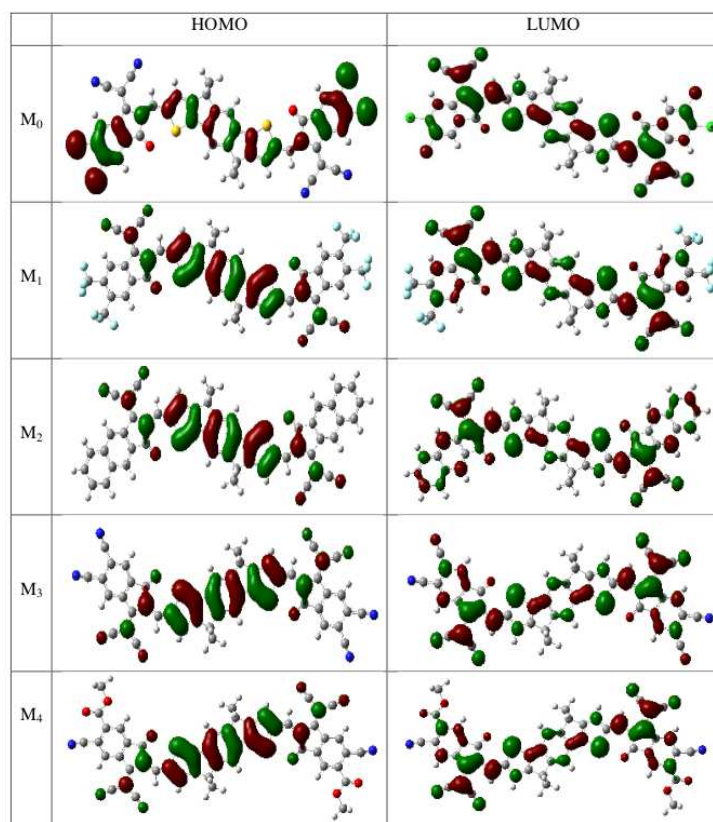


Figure 15: FMO isosurfaces calculated at the HSEH1PBE/6-311G(d,p)/PCM(chloroform) level.

is the field operator for the position of electron i . The charge-transfer number for an electron-hole excitation represents the overlap of the part of the hole on atom B with the part of the hole on atom A and so tells how much of an electron has been excited from atom A to atom B. Of course, Eq. (23) is incomplete until a way is specified to associate coordinates with atoms. As there is no unique way to do this, the exact evaluation of the charge-transfer numbers $\Omega_{A,B}$ depends upon particular choices of population analysis scheme^{55,81–84}. It may also be symmetrized⁵⁵ in which case it is the average of how much of an electron has been excited from A to B and how much has been excited from B to A. Calculated heat maps of S_1 TDMs are shown in **Fig. 16**. As should be expected from the FMO maps (Fig. 15), most of the HOMO \rightarrow LUMO excitation in these A-D-A molecules is from localized on D with a lesser extent on A. In this sense, D acts as the chromophore whose excitation is to be transferred to the A ends of the molecule. This charge transfer, already seen with the FMOs, is seen again by the presence of blue in the (D,A) and (A,D) blocks of the TDMs.

Neither the pictures of FMOs nor the TDM heat maps provide quantitative information about the electron-hole charge transfer. While many approaches have been proposed to characterize the degree of electron-hole separation, we will take a simple approach here by focusing on the oscillator strengths in Table 6 which are seen to be between about 2.5 and 3.0. Such large oscillator strengths are typical of charge transfer excitations. In fact, the transition dipole moment $\mu_{g,e} = eR_{g,e}$ for the excitation with energy $\hbar\omega$ may be calculated from the exact oscillator strength expression,

$$f = \frac{2\omega m_e}{3\hbar} e^2 R_{g,e}^2. \quad (24)$$

Values of $R_{g,e}$ (also shown in Table 6) provide a simple measure of electron-hole separation. We see that they are on the order of the size of one A unit or less consistent with physical expectations. The values of $R_{g,e}$ make it clear that **M₂** is the best molecule when it comes to maximizing electron-hole separation. It is also best in the sense of absorbing the most light.

We now wish to estimate solar cell performance with these candidate NFAs. We cannot do this with the original Scharber plot method^{15,16} (reviewed in the SI) because that assumes that light absorption only occurs in the DON, whereas we have used a detailed balance argument in Subsec. 3.1 to show that exciton formation due to light

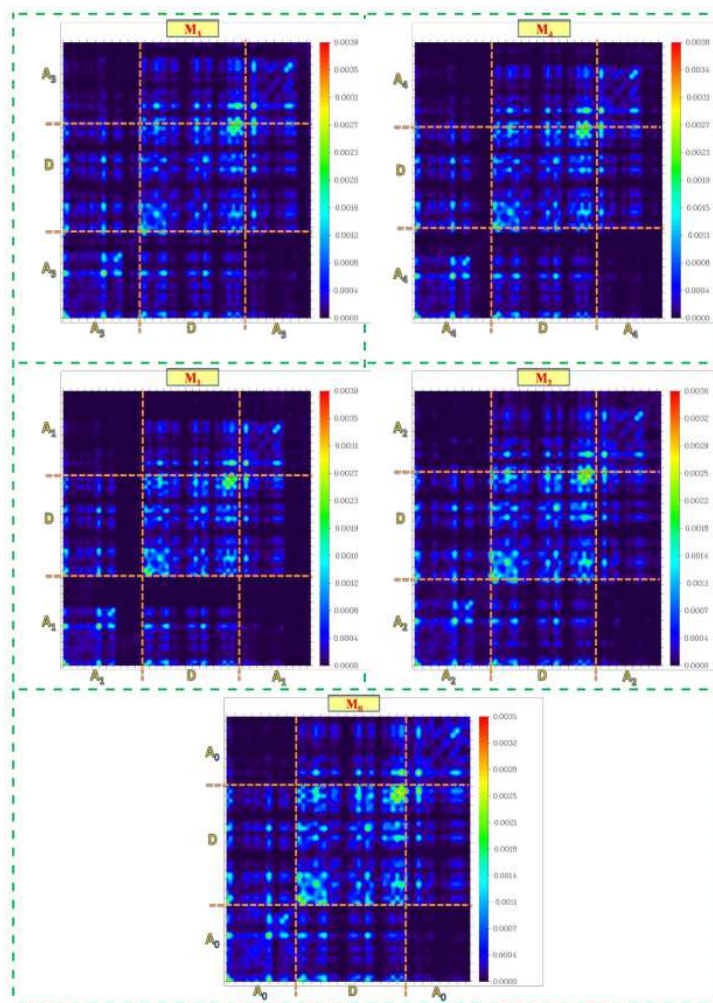


Figure 16: Heat maps of the S_1 excitation transition density matrices (TDMs) calculated at the TD-HSEH1PBE/6-311G(d,p)/PCM(chloroform) level using GAUSSIAN²⁹ and MULTIWFN^{54,55} where the charge-transfer numbers $\Omega_{A,B}$ have been calculated using Way 4 as described on page 211 of Ref.⁵⁵. Each pixel of the heat map is thus characterized by two atoms (A and B) and is symmetrized (the first equation at the top of page 211 of Ref.⁵⁵). As is usual, hydrogen atoms have been omitted from the figure in order to keep the size and complexity of the figure manageable. Note that no attempt has been made to insure that the atom numbering used in making the heat maps reflects the underlying symmetry of the molecule.

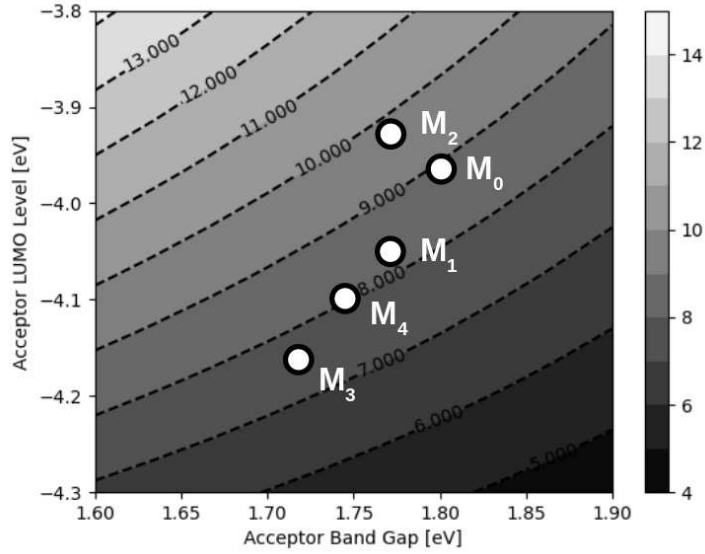


Figure 17: Scharber plot made using the finite width model.

ACC	eV_{oc} (eV)	J_{sc} (mA/cm ²)	PCE
ΔSCF			
M_0	0.79 eV	16.01 mA/cm ²	8.86 %
M_1	0.69 eV	16.76 mA/cm ²	8.10 %
M_2	0.83 eV	16.76 mA/cm ²	9.74 %
M_3	0.58 eV	18.28 mA/cm ²	7.42 %
M_4	0.66 eV	17.52 mA/cm ²	8.09 %
“Koopmans”			
M_0	0.76 eV	17.26 mA/cm ²	9.18 %
M_1	0.66 eV	18.02 mA/cm ²	8.33 %
M_2	0.81 eV	17.77 mA/cm ²	10.08 %
M_3	0.55 eV	19.58 mA/cm ²	7.54 %
M_4	0.63 eV	18.80 mA/cm ²	8.29 %

Table 8: Estimated PCEs for PM6:ACC cells obtained using Eq. (3) with $FF = 70\%$, $P_s = 99.971 \text{ mW.cm}^2$, Eq. (2) to calculate V_{oc} with $\delta = 0.74 \text{ eV}$, and Eq. (13) to calculate $J_{sc} = J_{fw}$ with $\Delta\lambda = 200 \text{ nm}$. The PM6 CV FMO energies are from Table 3 and the ACC CV FMO energies are from Table 4.

absorption must also be occurring in the ACC. Instead, we will make a Scharber plot for a PM6:ACC cell and our different candidate acceptors using the fw model introduced in Subsec. 3.1. **Figure 17** may be the first Scharber plot in the literature whose axes are labeled by the ACC gap and LUMO levels, instead of the usual DON quantities. It shows that the main factor influencing performance is the ACC LUMO level. **Table 8** provides specific numbers. These differ a bit depending upon whether the ACC FMO levels have been calculated using the ΔSCF CV FMO levels or the DFT FMO levels, but general trends are independent of which choice is made. The candidate ACC which is predicted to give the highest J_{sc} is **M₃** because it has the lowest HOMO-LUMO gap. However this is outweighed by eV_{oc} , the order of PCE of the different candidate ACCs being the same as the order of their eV_{oc} . The largest eV_{oc} , and hence the largest PCE, is for **M₂** because this molecule has the largest LUMO energy. Hence the energy of the photon exciting from the DON HOMO to the ACC LUMO is maximized and so is the energy needed for efficient charge separation. Figure 17 suggests that further progress could be made by lowering the ACC band gap while maintaining a high ACC LUMO energy.

4 Discussion and Conclusion

The advent of third generation bulk heterojunction OSCs is bringing OSC PCEs up to nearly 20%, making it possible to envisage OSCs moving out of niche markets to become an essential player in the evolving world of energy technology. OSCs use a DON:ACC architecture. First generation OSC design concentrated on P3HT:PC₆₁M-like OSCs where the major issue was cell morphology. The second generation mostly concentrated on replacing P3HT with more optimal donor compounds. The third and present generation consists of optimizing the ACC, replacing the PC₆₁M fullerene derivative with NFAs. These NFAs typically consist themselves of a push-pull architecture involving joined A and D units. They are typically flat molecules that stack well so as to form locally crystalline structures. This allows the rapid movement of charges away from the DON:ACC interface, hence minimizing electron-hole recombination and increasing cell performance. However too much crystallinity can also lead to undesirable OSC morphologies which decrease OSC performance. It has not been the purpose of this article to examine either morphologies or aggregation. Rather we begin with the known A-D-A ACC IDIC-4Cl and replace the

Cl end groups with other end groups making the reasonable assumption that such small changes will have little effect on morphology but will nevertheless affect the OSC PCE. It is to be emphasized that, while IDIC-4Cl does not yield PCEs of more than about 10%, the relatively simple A-D-A structure makes it possible to understand its performance in quite some detail. In particular, small structural variations are expected to lead to small variations in the corresponding PCE and we have analyzed the effects of these variations.

We began with an extensive validation in which we were able to confirm that the presence of side chains on IDIC-4Cl derivatives has little effect on core electronic properties. The molecules are rigid and geometry optimizations match well against the single crystal structure used for comparison purposes. Calculated CV FMOs agreed well with experiment. Recalculating using the same solvent as used in the experimental measurements further improves agreement between calculation and experiment. Absorption spectra calculated with TD-DFT were also in quite reasonable agreement with experiment. The DON:ACC OSC PCE was found to depend primarily on the J_{sc} which, somewhat surprisingly, does not simply increase as the ACC HOMO-LUMO gap increases. This is counter to what was found in second-generation OSCs where the short-circuit current generally follows the db model and always grows as the DON HOMO-LUMO gap increases. The difficulty was traced back to the need to take into account light absorption in both the DON and ACC materials. We have modeled this by introducing a fw approximation into Scharber's theory for estimating OSC PCE performance. In Scharber's plots PCE increases with both the DON HOMO-LUMO gap and the DON LUMO energy. In our fw theory, PCE increases with the ACC LUMO energy but actually decreases as the ACC HOMO-LUMO gap grows and approaches the DON HOMO-LUMO gap. Our theory is very simple, though adequate for present purposes.

The rough effects of electron donation and electron accepting groups on the HOMO and LUMO energies and on the HOMO-LUMO gap is well established in FMO theory. Determining the relative strength of electron acceptors is not always *a priori* obvious, especially when electron acceptors are of similar strength. We have used conceptual DFT to calculate electrophilicity indices and showed that the CV FMO energies and the CV HOMO-LUMO gap all tend to decrease as the electrophilicity index increases. These results were confirmed by showing that the trends match very well both the classic theory

of Hammett but also the newer theory of Remya and Suresh. Our finite-width model predicts that the DON:ACC OSC PCE will be especially sensitive to the ACC LUMO energy, with the ACC having the highest LUMO energy giving the highest PCE. We thus predict that only one of the four candidate ACC molecules will outperform the original ACC molecule and have understood why the other candidate molecules should have lower PCEs. This same candidate ACC molecule also has the largest oscillator strength for the important $^1(\text{HOMO,LUMO})$ charge-transfer transition and the charge transfer is shown to be more delocalized than for the other molecules studied here.

Acknowledgments

It is both appropriate and a pleasure to have this article appear in a volume honoring Carlo Adamo on the occasion of his 60th birthday. Carlo has made important contributions in many areas of methodology used in the present paper, including the development of density-functional approximations, implicit solvent models, and simulations of photo-processes.

We would like to thank Pierre Girard, Denis Charapoff, Sébastien Morin, and for technical support in the context of the Grenoble *Centre d'Experimentation du Calcul Intensif en Chimie (CECIC)* computers used for the calculations reported here. Mourad Chemek, Tarek Mestiri, and Malak Hijazi are thanked for helpful discussions.

Author Contributions

Author credit has been assigned using the CRediT contributor roles taxonomy system⁸⁵.

Walid Taouali: Conceptualization, investigation, formal analysis, writing - original draft, visualisation.

Kamel Alimi: Writing - review & editing.

Asma Sindhoo Nangraj: Visualisation, software.

Mark E. Casida: Supervision, resources, formal analysis, writing - original draft, visualisation, software.

Conflicts of Interest

The authors declare no conflict of interest.

Supplementary Information

1. Scharber Plots
2. Chemical Names
3. Optimized Structures
4. FMO theory diagram
5. Spectral shift

References

1. Karki, A.; Gillett, A. J.; Friend, R. H. and Nguyen, T. Q., *Adv. Energy Mater.*, 2020, **11**, 2003441.
2. Liu, Q.; Jiang, Y.; Jin, K.; Qin, J.; Xu, J.; Li, W.; Xiong, J.; Liu, J.; Xiao, Z.; Sun, K.; Yang, S.; Zhang, X. and Ding, L., *Sci. Bull.*, 2020, **65**, 272.
3. Lin, Y.; Firdaus, Y.; Isikgor, F. H.; Nugraha, M. I.; Yengel, E.; Harrison, G. T.; Hallani, R.; El-Labban, A.; Faber, H.; Ma, C.; Zheng, X.; Subbiah, A.; Howells, C. T.; Bakr, O. M.; McCulloch, I.; Wolf, S.; Tsetseris, L. and Anthopoulos, T. D., *ACS Energy Lett.*, 2020, **5**, 2935.
4. Zhang, G.; Lin, F. R.; Qi, F.; Meumüller, T.; Distler, A.; Egelhaaf, H.; Li, N.; Chow, P. C. Y.; Brabec, C. J.; Jen, A. K.; and Yip, H., *Chem. Rev.*, 2022, **122**, 14180.
5. Giebink, N. C.; Wiederrecht, G. P.; Wasielewski, M. and Forrest, S. R., *Phys. Rev. B*, 2010, **82**, 155305.
6. Giebink, N. C.; Lassiter, B. E.; Wiederrecht, G. P.; Wasielewski, M. R. and Forrest, S. R., *Phys. Rev. B*, 2010, **82**, 155306.
7. Wagner, J.; Gruber, M.; Wilke, A.; Tanaka, Y.; Topczak, K.; Steindamm, A.; Hörmann, U.; Optiz, A.; Nakayama, Y.; Ishii, H.; Pflaum, J.; Koch, N. and Brütting, W., *J. Appl. Phys.*, 2012, **111**, 054509.
8. Huh, Y. H.; Park, B. and Hwang, I., *J. Appl. Phys.*, 2014, **115**, 124504.
9. Giannini, S.; Carof, A.; Ellis, M.; Yang, H.; Ziogos, O. G.; Ghosh, S. and Blumberger, J., *Nat. Commun.*, 2019, **10**.

10. Giannini, S.; Ziogos, O. G.; Carof, A.; Ellis, M. and Blumberger, J., *Adv. Theory Simul.*, 2020, **3**, 2000093.
11. Clarke, T. M. and Durrant, J. R., *Chem. Rev.*, 2010, **110**, 6736.
12. Ismail, Y. A. M.; Soga, T. and Jimbo, T., *J. Appl. Phys.*, 2011, **109**, 103109.
13. Street, R. A.; Song, K. W.; Northrup, J. E. and Cowan, S., *Phys. Rev. B*, 2011, **83**, 165207.
14. Nojima, H.; Kobayashi, T.; Nagase, T. and Naito, H., *Nature*, 2019, **9**, 20346.
15. Scharber, M. C.; Muhlbacher, D.; Koppe, M.; Denk, P.; Waldouf, C.; Heeger, A. J. and Brabec, C. J., *Adv. Mater.*, 2006, **18**, 789.
16. Scharber, M. C., *Adv. Mater.*, 2016, **28**, 1994.
17. Liu, G.; Jia, J.; Zhang, K.; Jia, X.; Yin, Q.; Zhong, W.; Li, L.; Huang, F. and Cao, Y., *Adv. Energy Mater.*, 2019, **9**, 1803657.
18. Zhu, C.; Yuan, J.; Cai, F.; Meng, L.; Zhang, H.; Chen, H.; Li, J.; Qiu, B.; Peng, H.; Chen, S.; Hu, Y.; Yang, C.; Gao, G.; Zou, Y. and Li, Y., *Energy Environ. Sci.*, 2020, **13**, 2459.
19. Yi, X.; Ho, C. H. Y.; Gautam, B.; Lei, L.; Chowdhury, A. H.; Bahrami, B.; Qiao, Q. and So, F., *J. Mater. Chem. C*, 2020, **8**, 16092.
20. Li, C.; Yue, Q.; Wu, H.; Li, B.; Fan, H. and Zhu, X., *J. Energy Chem.*, 2021, **52**, 60.
21. Ke, X.; Meng, L.; Wan, X.; Cai, Y.; Gao, H.; Yi, Y. Q. Q.; Guo, Z.; Zhang, H.; Li, C. and Chen, Y., *Nano Energy*, 2020, **75**, 104988.
22. Damas, G. B.; Kieseritzky, F.; Hellberg, J.; Marchiori, C. F. N. and Araujo, C. M., *J. Phys. Chem. C*, 2019, **123**, 30799.
23. Huang, Y.; Zhou, W.; Li, X.; Li, J. and Song, Y., *Mater. Adv.*, 2021, **2**, 2097.
24. Zhang, Y.; Zhang, C.; Huang, H.; Jin, H.; Gao, Y.; Zheng, R.; Song, J.; Li, C.; Ma, Z. and Bo, Z., *Dyes Pigm.*, 2021, **184**, 108789.
25. Khalida, A.; Khera, R. A.; Saeed, A.; Khalid, M.; Iqbal, S. and Iqbal, J., *Optik*, 2021, **228**, 166138.
26. Yousaf, I.; Khera, R. A.; Iqbal, J.; Gul, S.; Jabeen, S.; Ihsan, A. and Ayub, K., *Mater. Sci. Semicond. Process*, 2021, **121**, 105345.
27. Lee, T.; Song, C. E.; Lee, S. K.; Shin, W. S. and Lim, E., *ACS Omega*, 2021, **6**, 4562.
28. Qu, J.; Chen, H.; Zhou, J.; Lai, H.; Liu, T.; Chao, P.; Li, D.; Xie, Z.; He, F. and Ma, Y., *ACS Appl. Mater. Interfaces*, 2018, **10**, 39992.

29. Frisch, M. J.; Trucks, G. W.; Schlegel, H. B.; Scuseria, G. E.; Robb, M. A.; Cheeseman, J. R.; Scalmani, G.; Barone, V.; Mennucci, B.; Petersson, G. A.; Nakatsuji, H.; Caricato, M.; Li, X.; Hratchian, H. P.; Izmaylov, A. F.; Bloino, J.; Zheng, G.; Sonnenberg, J. L.; Hada, M.; Ehara, M.; Toyota, K.; Fukuda, R.; Hasegawa, J.; Ishida, M.; Nakajima, T.; Honda, Y.; Kitao, O.; Nakai, H.; Vreven, T.; Montgomery, Jr., J. A.; Peralta, J. E.; Ogliaro, F.; Bearpark, M.; Heyd, J. J.; Brothers, E.; Kudin, K. N.; Staroverov, V. N.; Kobayashi, R.; Normand, J.; Raghavachari, K.; Rendell, A.; Burant, J. C.; Iyengar, S. S.; Tomasi, J.; Cossi, M.; Rega, N.; Millam, J. M.; Klene, M.; Knox, J. E.; Cross, J. B.; Bakken, V.; Adamo, C.; Jaramillo, J.; Gomperts, R.; Stratmann, R. E.; Yazyev, O.; Austin, A. J.; Cammi, R.; Pomelli, C.; Ochterski, J. W.; Martin, R. L.; Morokuma, K.; Zakrzewski, V. G.; Voth, G. A.; Salvador, P.; Dannenberg, J. J.; Dapprich, S.; Daniels, A. D.; Farkas, O.; Foresman, J. B.; Ortiz, J. V.; Cioslowski, J. and Fox, D. J., *GAUSSIAN 09* Revision D.01, 2009.
30. Tomasi, J.; Mennucci, B. and Cammi, R., *Chem. Rev.*, 2005, **105**, 2999.
31. Heyd, J. and Scuseria, G., *J. Chem. Phys.*, 2004, **121**, 1187.
32. Krishnan, R.; Binkley, J. S.; Seeger, R. and Pople, J. A., *J. Chem. Phys.*, 1980, **72**, 650–654.
33. McLean, A. D. and Chandler, G. S., *J. Chem. Phys.*, 1980, **72**, 5639–5648.
34. Francl, M. M.; Pietro, W. J.; Hehre, W. J.; Binkley, J. S.; Gordon, M. S.; DeFrees, D. J. and Pople, J. A., *J. Chem. Phys.*, 1982, **77**, 3654–3665.
35. Stephens, P. J.; Devlin, F. J.; Chabalowski, C. F. and Frisch, M. J., *J. Phys. Chem.*, 1994, **98**, 11623.
36. Adamo, C. and Barone, V. J., *Chem. Phys.*, 1999, **110**, 6158.
37. Perdrew, J. P. and Wang, Y., *J. Phys. Rev.*, 1992, **45**, 13244.
38. Dennington, R.; Keith, T. and Millam, J., *GAUSS VIEW*, version 5, 2009.
39. Schaftenaar, B., *MOLDEN: A pre- and post processing program of molecular electronic structure* <https://www3.cmbi.umcn.nl/molden/>.
40. Darghouth, A. M. H. M.; Correa, G. C.; Juillard, S.; Casida, M. E.; Humeniuk, A. and Mitrić, R., *J. Chem. Phys.*, 2018, **149**, 134111.
41. Oxtoby, D. W.; Gillis, H. P. and Campion, A., *Principles of Modern Chemistry, 7th Edition*, Brooks/Cole CENGAGE Learning, Singapore, 2008.
42. Peljo, P. and Girault, H. H., *Energy Environ. Sci.*, 2018, **11**, 2306.
43. Namazian, M.; Lin, C. Y. and Coote, M. L., *J. Chem. Theory Comput.*, 2010, **6**, 2721.
44. Kohn, W. and Sham, L. J., *Phys. Rev.*, 1965, **140**, A1133.
45. Casida, M. E., *Phys. Rev. B*, 1999, **59**, 4694.
46. Perdew, J. P. and Levy, M., *Phys. Rev. Lett.*, 1983, **51**.

47. Sham, L. J. and Schlüter, M., *Phys. Rev. Lett.*, 1983, **51**.
48. Koopmans, T., *Physica*, 1934, **1**, 104.
49. Baer, R.; Livshits, E. and Salzner, U., *Annu. Rev. Phys. Chem.*, 2010, **61**, 85.
50. Hamel, S.; Casida, M. E. and Salahub, D. R., *J. Chem. Phys.*, 2002, **116**, 8276.
51. Hamel, S.; Duffy, P.; Casida, M. E. and Salahub, D. R., *J. Electr. Spectr. and Related Phenomena*, 2002, **123**, 345.
52. Darghouth, A. A. M. H. M.; Casida, M. E.; Taouali, W.; Alimi, K.; Ljungberg, M. P.; Koval, P.; Sánchez-Portal, D. and Foerster, D., *Computation*, 2015, **3**, 616.
53. Goelsky, S. I., [SWIZARD program](http://www.sgchem.net) <http://www.sgchem.net>, University of Ottawa, Ottawa, Canada, 2013.
54. Lu, T. and Chen, F., *J. Comput. Chem.*, 2012, **33**, 580.
55. Lu, T., MULTIWFN — A multifunctional wavefunction analyzer — Software manual with tutorials and abundant examples, 24 august 2020 http://sobereva.com/multiwfn/misc/Multiwfn_3.7.pdf.
56. Huang, Z.; Zhou, R.; Lv, M.; Zhang, H.; Yang, C.; Shi, Y.; Tang, Y.; Zhang, J.; Lu, K. and Wei, Z., *Mater. Chem. Front.*, 2021, **5**, 1405.
57. Lin, Y.; He, Q.; Zhao, F.; Huo, L.; Mai, J.; Lu, X. and ..., , *J. Am. Chem. Soc.*, 2016, **138**, 2973.
58. Wu, Q.; Deng, D.; Zhou, R.; Zhang, J.; Zou, W.; Liu, L.; Wu, S.; Lu, K. and Wei, Z., *ACS Appl. Mater. Interfaces*, 2020, **12**, 25100.
59. Zhang, Z.; Wu, Q.; Deng, D.; Zhang, J. and Wei, Z., *J. Mater. Chem. C*, 2020, **8**, 15385.
60. Li, X.; Meng, H.; Shen, F.; Su, D.; Huo, S.; Shan, J.; Huang, J. and Zhana, C., *Dyes Pigm.*, 2019, **166**, 196.
61. Becke, A. D., *J. Chem. Phys.*, 1993, **98**, 5648.
62. Vosko, S. H.; Wilk, L. and Nusair, M., *Can. J. Phys.*, 1980, **58**, 1200.
63. Rohatgi, A., WEBPLOTDIGITIZER: Web based tool to extract data from plots, images, and maps <https://apps.automeris.io/WebPlotDigitizer/>, 2021.
64. Shockley, W., *Electrons and Holes in Semiconductors with Applications to Transistor Electronics*, D. Van Nostrand Company, New York City, 1950.
65. Singh, J., *Semiconductor Devices: Basic Principles*, John Wiley and Sons, New York City, 2001.
66. Mihailetchi, V. D.; Blom, P. W. M.; Hummelen, J. C. and Rispens, M. T., *J. Appl. Phys.*, 2003, **94**, 6849.

67. Roa Díaz, S., *Physica B*, 2022, **624**, 413427.
68. Shockley, W. and Queisser, H. J., *J. Appl. Phys.*, 1961, **32**, 510.
69. Alharbi, F. H.; Rashkeev, S. N.; El-Mellouhi, F.; Lüthi, H. P.; Tabet, N. and Kais, S., *npj Comput. Mater.*, 2015, **1**, 15003.
70. Reference air mass 1.5 spectra <https://www.nrel.gov/grid/solar-resource/spectra-am1.5.html>.
71. Lin, Y.; Wang, J.; Zhang, Z.; Bai, H.; Li, Y.; Zhu, D. and Zhan, X., *Adv. Mater.*, 2015, **27**, 1170.
72. Lin, Y.; Z.-G. Zhang, ; Bai, H.; Wang, J.; Yao, Y.; Li, Y.; Zhu, D. and Zhan, X., *Energy Environ. Sci.*, 2015, **8**, 610.
73. Liu, S., *Conceptual Density Functional Theory: Towards a New Chemical Reactivity Theory, Volumes 1 and 2*, Wiley-VCH, Weinheim, Germany, 2022.
74. Fleming, I., *Frontier Orbitals and Organic Chemical Reactions*, John Wiley and Sons, New York, 1976.
75. Anh, N. T., *Frontier Orbitals: A Practical Manual*, John Wiley and Sons, The Atrium, Southern Gate, Chichester, West Sussex PO19 8SQ, England, 2007.
76. Parr, R. G.; Szentpaly, L. V. and Liu, S. B., *J. Am. Chem. Soc.*, 1999, **121**, 1922.
77. Hansch, C.; Leo, A. and Taft, R. W., *Chem. Rev.*, 1991, **91**, 165.
78. Remya, G. S. and Suresh, C. H., *Phys. Chem. Chem. Phys.*, 2016, **18**, 20615.
79. Jones, R. A. Y., *Physical and Mechanistic Organic Chemistry*, Cambridge University Press, Cambridge, England, 1979.
80. Casida, M. E. In *Recent Advances in Density Functional Methods*, Chong, D. P., Ed.; World Scientific, Singapore, 1995; page 155.
81. Plasser, F. and Lischka, H., *J. Chem. Theory Comput.*, 2012, **8**, 2777.
82. Plasser, F.; Bäppler, S. A.; Wormit, M. and Dreuw, A., *J. Chem. Phys.*, 2014, **141**, 024107.
83. Plasser, F.; Wormit, M. and Dreuw, A., *J. Chem. Phys.*, 2014, **141**, 024106.
84. Plasser, F., *J. Chem. Phys.*, 2020, **152**, 084108.
85. Credit (contributor roles taxonomy) <https://credit.niso.org/>.

Supplementary Information for “Density-Functional Theory (DFT) and Time-Dependent DFT Study of the Chemical and Physical Origins of Key Photoproperties of End-Group Derivatives of the Nonfullerene Bulk Heterojunction Organic Solar Cell Acceptor Molecule IDIC

Taouali W*, Alimi K*, Nangraj A.S. †, Casida M.E.‡

Contents

1	Scharber Plots	1
2	Chemical Names	5
3	Optimized Structures	6
4	FMO theory diagram	26
5	Spectral Shift	27

1 Scharber Plots

We wrote our own computer program to make “Scharber plots” (also known as “Scharber diagrams”)¹. We review the basic theory as we had to clarify certain points in the original description of the phenomenological theory² in order to be able to write our own computer program. Note that this allows us to apply the same basic ideas more widely than did Scharber should we wish to do so. *Key assumptions are given in italics.*

Experimentalists who seek to characterize a new material for potential use in a solar cell, generally illuminate the cell with AM 1.5 G light (solar spectrum at ground level as

*Laboratoire de Recherche (LR18ES19), Synthèse Asymétrique et Ingénierie Moléculaire de Matériaux Organiques pour l’Électroniques Organiques, Faculté des Sciences de Monastir, Université de Monastir, 5000 Monastir, TUNISIA

†State Key Laboratory of Microbial Metabolism, Shanghai Jiao Tong University, Shanghai, CHINA

‡Laboratoire de Spectrométrie, Interactions et Chimie théorique (SITh), Département de Chimie Moléculaire (DCM, UMR CNRS/UGA 5250), Institut de Chimie Moléculaire de Grenoble (ICMG, FR2607), Université Grenoble Alpes (UGA) 301 rue de la Chimie, BP 53, F-38041 Grenoble Cedex 9, FRANCE

seen through an air mass of 1.5 times that of the atmosphere) and power P_s . They then make a (V, J) -plot whose general form is usually well described by the Shockley diode equation³. When the voltage $V = 0$, then we obtain the short-circuit current density J_{sc} (mA/cm²). When the current density $J = 0$, then we obtain the open-circuit voltage V_{oc} (V). Inscribing a square inside the (V, J) -curve defines the point (V_m, J_m) . Since the product $J_m V_m$ is also the maximum power that can be extracted from the solar cell, the power conversion efficiency (PCE) of the solar cell is,

$$\eta = \frac{V_m J_m}{P_s}. \quad (1)$$

Shockley and Queisser showed for a simple solar cell that η has a thermodynamic upper limit⁴ which today is accepted to be 34% at AM 1.5G. Organic solar cells are significantly less efficient.

Another quantity that may be determined from a (V, J) -plot is the fill factor (FF), given by

$$\text{FF} = \frac{V_m J_m}{V_{oc} J_{sc}}. \quad (2)$$

According to Grätzel⁵, “The value of the fill factor reflects the extent of electrical (Ohmic) and electrochemical (overvoltage) losses.” *In constructing the Scharber plot, we use a typical value of $\text{FF} = 0.65$.* Combining Eqs. (1) and (2) gives,

$$\eta = \frac{J_{sc} V_{oc} \text{FF}}{P_s}, \quad (3)$$

For good electrical contacts, the open-circuit voltage is almost given by just the difference of the CV HOMO energy of the molecules making up the acceptor layer $\epsilon_{\text{HOMO}}^{\text{DON}}$ and of the CV LUMO energy $\epsilon_{\text{LUMO}}^{\text{ACC}}$ of the molecules making up the donor layer. It can be shown that,

$$eV_{oc} \leq \epsilon_{\text{LUMO}}^{\text{ACC}} - \epsilon_{\text{HOMO}}^{\text{DON}}, \quad (4)$$

with near equality obtained for good (ohmic) contacts between the solar cell and the electrodes. Empirically for a number of polymer heterojunction solar cells where the acceptor molecule is PCBM, near equality is found — that is,

$$V_{oc} = \frac{1}{e} \left(\epsilon_{\text{LUMO}}^{\text{PCBM}} - \epsilon_{\text{HOMO}}^{\text{DON}} \right) - 0.3 \text{ V}. \quad (5)$$

This is a second assumption used in constructing the Scharber plot. Equation (5) is “Equation 1 for V_{oc} ” in Ref.². We note that the original Scharber plot used

$$\epsilon_{\text{LUMO}}^{\text{PCBM}} = -4.3 \text{ eV}, \quad (6)$$

which is another assumption used in making the Scharber plot. (For comparison, recall that others^{6,7} have reported that the PCBM CV LUMO is located at $-3.83 \pm 0.15 \text{ eV}$ ⁶.)

The penultimate quantity needed to be able to construct the Scharber plot is J_{oc} . *This is obtained by making the two detailed balance assumptions*, namely: (i) every photon whose energy is greater than the fundamental gap,

$$E_g = \epsilon_{\text{LUMO}}^{\text{Donor}} - \epsilon_{\text{HOMO}}^{\text{Donor}}, \quad (7)$$

is absorbed and (ii) every absorbed photon creates an electron-hole pair⁴. *In constructing the Scharber plot, it is assumed that the external quantum efficiency EQE = 65% — i.e., that only 65% of the photons are absorbed.* We may then convert AM 1.5 Global data into a current density. This is complicated by the fact that the data is reported as a spectral irradiance in units of watts/(m².nm). To see how to do the calculation, consider first monochromatic light of wave length λ hitting an area A during a time Δt . Let N be the number of photons hitting during this time. Then the current density is just,

$$J = \frac{eN}{A\Delta t}. \quad (8)$$

The irradiance (\mathcal{I}) is the energy per area per time. So,

$$\mathcal{I} = \frac{E}{A\Delta t} = \frac{N h \nu}{A\Delta t} = \frac{N h c}{A\Delta t \lambda}. \quad (9)$$

Hence,

$$J = e \frac{\mathcal{I} \lambda}{h c}. \quad (10)$$

However AM 1.5G light is not monochromatic, so we must write that,

$$J = \frac{e}{A\Delta t} \int_0^{\lambda_g} dN(\lambda), \quad (11)$$

where the gap wavelength is,

$$\lambda_g = \frac{h c}{E_g} = \frac{1240 \text{ eV.nm}}{E_g}. \quad (12)$$

The spectral irradiance $F(\lambda)$ is defined as,

$$F(\lambda) = \frac{d\mathcal{I}(\lambda)}{d\lambda}, \quad (13)$$

so the irradiance for a small wavelength interval $(\lambda, \lambda + \Delta\lambda)$ is,

$$F(\lambda)d\lambda = d\mathcal{I}(\lambda) = \frac{h c}{A\Delta t} \frac{1}{\lambda} dN(\lambda). \quad (14)$$

Then,

$$dN(\lambda) = F(\lambda) \lambda \frac{A\Delta t}{h c} d\lambda, \quad (15)$$

and,

$$J = \frac{e}{h c} \int_0^{\lambda_g} F(\lambda) \lambda d\lambda. \quad (16)$$

It remains only to calculate the constant e/hc in appropriate units:

$$\frac{e}{h c} = \frac{(1.602 \times 10^{-19} \text{ C})(10^{+3} \text{ mA}/(\text{C/s}))}{(6.626 \times 10^{-34} \text{ J.s})(2.998 \times 10^8 \text{ m/s})(10^2 \text{ cm/m})^2(10^9 \text{ nm/m})} = 8.0645 \times 10^{-5} \frac{\text{mA.m}^2}{\text{W.cm}^2.\text{nm}}. \quad (17)$$

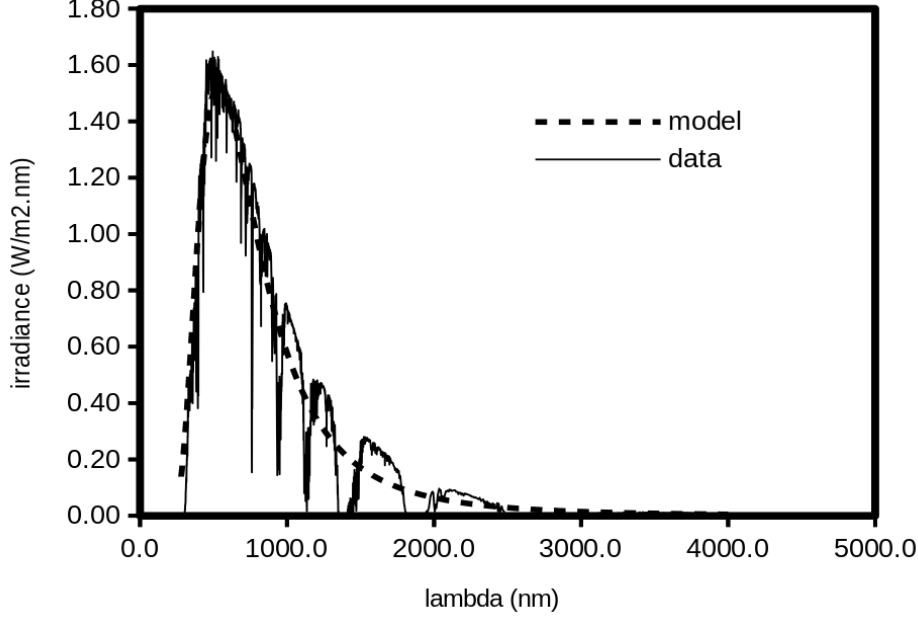


Figure 1: Comparison of the model spectral irradiance $F3(\lambda)$ obtained from Eq. (18) via Eq. (16) with AM 1.5 G spectra irradiance data $F(\lambda)$ from Ref.⁹.

We have carried out the integration using a spreadsheet and we have found it to be very well approximated by the formula,

$$J3(E_g) = (73.531 \text{ mA/cm}^2) e^{-(0.440)(E_g/\text{eV})^{1.8617}}, \quad (18)$$

given as Eq. (5) of Ref.⁸. Conversely, we may obtain an estimate $F3(\lambda)$ of the irradiance $F(\lambda)$ by taking the derivative of Eq. (16) to obtain,

$$F3(\lambda) = \frac{hc}{e\lambda} \frac{dJ3(hc/\lambda)}{d\lambda}. \quad (19)$$

Figure 1 shows that $F3$ is a reasonable smoothed approximation to the standard AM 1.5 G irradiance data⁹.

And the very last quantity that we need is the total power of the sun, P_s . This can be obtained by directly integrating the AM 1.5G solar data,

$$P_s = \int_0^\infty F(\lambda) d\lambda = 999.71 \text{ W/m}^2 = 99.971 \text{ mW/cm}^2. \quad (20)$$

Combining all of the assumptions underlying the Scharber model into a single formula then gives,

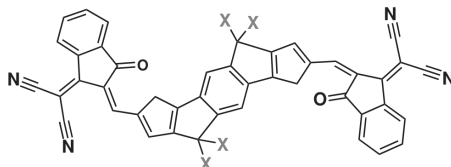
$$\eta = 100\% \times \frac{0.65 J3(E_g)}{99.971 \text{ mW.cm}^2} \left[\frac{1}{e} \left(\epsilon_{\text{LUMO}}^{\text{PCBM}} - \epsilon_{\text{HOMO}}^{\text{DON}} \right) - 0.3 \text{ V} \right] (0.65). \quad (21)$$

We note that we have verified that our program gives Scharber plots in perfect agreement with plots in the original published work². Moreover mastery of the Scharber formalism allows the same formalism to be generalized to other contexts when, say, an exact FF is known experimentally or the PCBM is replaced with a different ACC as is done in the present work.

2 Chemical Names

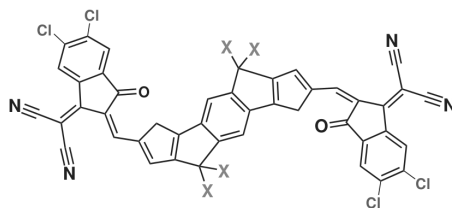
It is common in this field to use abbreviations rather than long chemical names. Moreover the same abbreviations are frequently reused for the same molecules differing only by the nature of their side groups. The full names and Lewis representations are given here for molecules referred to only by abbreviations in the main text.

IDIC The generic structure is



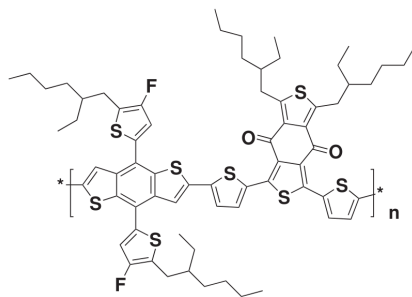
and has the name 2,2'-((2Z,2'Z)-((4,4,9,9-X-4,9-dihydro-s-indaceno[1,2-b:5,6-b']dithiophene-2,7-diyl)bis(methanylylidene))bis(3-oxo-2,3-dihydro-1H-indene-2,1-diylidene))dimalononitrile where X stands for four equivalent groups. When we want to be more specific, then we will write IDIC(X). For example, X should be replaced by “tetrahexyl” in the original IDIC¹⁰, by “tetraoctyl” in Ref.¹¹, by “tetrakis(4-hexylphenyl)” in the compound IDIC-4H of Ref.¹², and by “tetramethyl” for the simplified model compound for which calculations are actually done in this paper.

IDIC-4Cl The generic structure is



and has the name 2,2'-((2Z,2'Z)-((4,4,9,9-X-4,9-dihydro-s-indaceno[1,2-b:5,6-b']dithiophene-2,7-diyl)bis(methanylylidene))bis(5,6-dichloro-3-oxo-2,3-dihydro-1H-indene-2,1-diylidene))dimalononitrile where X stands for four equivalent groups. When we want to be more specific, then we will write IDIC(X)-4Cl. For example, X should be replaced by “tetrahexyl” in the original IDIC-4Cl¹³, by “tetraoctyl” by the compound in Refs.^{11,14,15}, by “tetrakis(4-hexylphenyl)” in the compound in Ref.¹², and by “tetramethyl” for the simplified model compound for which calculations are actually done in this paper.

PM6 poly[(2,6-(4,8-bis(5-(2-ethylhexyl-3-fluoro)thiophen-2-yl)-benzo[1,2-b:4,5-b']-dithiophene))-*alt*-(5,5-(1',3'-di-2-thienyl-5',7'-bis(2-ethylhexyl)benzo[1',2'-c:4',5'-c']dithiophene-4,8-dione))]



3 Optimized Structures

In this appendix, we give the (x, y, z) -coordinates in Ångströms of our optimized geometries. First are the geometries optimized at the HSEH1PBE/6-311G(d,p)/PCM level. Each geometry is followed by a table with the ten lowest vibrational frequencies *after* projecting out translations and rotations.

Optimized Geometries and Frequencies in Chloroform

M ₀ (simplified model of IDIC-4Cl)							
Optimized Geometry in Chloroform							
Atom (No.)	<i>x</i>	<i>y</i>	<i>z</i>	Atom (No.)	<i>x</i>	<i>y</i>	<i>z</i>
C(1)	-5.057198	1.366294	-0.018172	H(41)	-1.347859	2.725303	-2.238766
S(2)	-4.265293	-0.209939	0.018629	H(42)	4.406826	-3.440816	0.074379
C(3)	-2.735637	0.549772	-0.006033	H(43)	1.328323	-2.856013	-2.089611
C(4)	-2.799539	1.938500	-0.043460	H(44)	1.827425	-4.282161	-1.160868
C(5)	-4.104005	2.400601	-0.049474	H(45)	0.129976	-3.783035	-1.167815
C(6)	-1.414543	2.540192	-0.066420	H(46)	0.140701	-3.704786	1.386352
C(7)	-1.368187	0.108000	0.001295	H(47)	1.837929	-4.205267	1.394087
C(8)	-0.564174	1.275400	-0.033008	H(48)	1.348034	-2.725076	2.239507
C(9)	-0.811539	-1.175020	0.034882	H(49)	6.571199	-2.749882	0.032753
C(10)	0.564177	-1.275357	0.033729	H(50)	11.892811	-1.012335	0.012473
C(11)	1.368187	-0.107960	-0.000581	H(51)	9.012695	3.050525	-0.001739
C(12)	0.811538	1.175062	-0.034164	O(52)	6.721430	1.332424	-0.019150
C(13)	-1.160088	3.416166	1.167652	C(53)	9.376014	-2.741232	-0.034255
C(14)	-1.170742	3.340147	-1.353175	C(54)	8.510400	-3.866563	-0.060873
C(15)	2.735639	-0.549733	0.006675	C(55)	10.745752	-3.115239	-0.038057
C(16)	1.414546	-2.540149	0.067135	N(56)	7.847863	-4.814003	-0.084083
C(17)	2.799538	-1.938460	0.044071	N(57)	11.846248	-3.469332	-0.041673
S(18)	4.265295	0.209978	-0.018096	C(58)	-6.432142	1.674305	-0.013252
C(19)	5.057199	-1.366266	0.018538	H(59)	-6.571207	2.749891	-0.032661
C(20)	4.104006	-2.400565	0.049938	C(60)	-7.586066	0.922381	0.007852
C(21)	1.159983	-3.416226	-1.166832	C(61)	-8.948286	1.430855	0.012573
C(22)	1.170849	-3.339999	1.353986	C(62)	-7.650251	-0.547405	0.012935
C(23)	6.432139	-1.674296	0.013379	C(63)	-9.852347	0.260342	0.001758
C(24)	7.586062	-0.922383	-0.007887	C(64)	-9.376049	2.741218	0.033514
C(25)	8.948275	-1.430871	-0.012956	C(65)	-9.081609	-0.905487	0.004765
C(26)	7.650261	0.547399	-0.012812	O(66)	-6.721423	-1.332428	0.019558
C(27)	9.852352	-0.260370	-0.002147	C(67)	-11.237492	0.153687	-0.009041
C(28)	9.081621	0.905469	-0.004859	C(68)	-10.745790	3.115211	0.036832
C(29)	11.237499	-0.153723	0.008470	C(69)	-8.510452	3.866558	0.060188
C(30)	11.813608	1.114268	0.015581	C(70)	-9.638135	-2.166097	-0.001155
C(31)	11.023780	2.273151	0.011502	C(71)	-11.813595	-1.114307	-0.016049
C(32)	9.638156	2.166073	0.001148	H(72)	-11.892804	1.012298	-0.013248
H(33)	-4.406834	3.440848	-0.073985	N(73)	-11.846290	3.469294	0.040040
H(34)	-1.445315	-2.055334	0.060661	N(74)	-7.847930	4.814008	0.083425
H(35)	1.445321	2.055372	-0.059946	C(75)	-11.023756	-2.273184	-0.011705
H(36)	-1.328514	2.855869	2.090365	H(76)	-9.012666	-3.050542	0.001944
H(37)	-0.130078	3.782970	1.168762	Cl(77)	-11.740213	-3.840915	-0.019663
H(38)	-1.827530	4.282100	1.161701	Cl(78)	-13.535205	-1.223345	-0.030374
H(39)	-1.837809	4.205426	-1.393259	Cl(79)	11.740246	3.840875	0.019539
H(40)	-0.140589	3.704929	-1.385430	Cl(80)	13.535223	1.223290	0.029698

M_0 (simplified model of IDIC-4Cl)			
Lowest Vibrational Frequencies in Chloroform			
Vibration Number	Frequency	Vibration Number	Frequency
1	4.150 cm^{-1}	6	23.890 cm^{-1}
2	4.520 cm^{-1}	7	33.150 cm^{-1}
3	6.650 cm^{-1}	8	37.380 cm^{-1}
4	15.310 cm^{-1}	9	38.690 cm^{-1}
5	17.700 cm^{-1}	10	39.200 cm^{-1}

The largest magnitude imaginary frequency before projecting out the vibrations and rotations was $8.9994i \text{ cm}^{-1}$.

M₁ (simplified model of IDIC-4CF₃)

Optimized Geometry in Chloroform

Atom (No.)	<i>x</i>	<i>y</i>	<i>z</i>	Atom (No.)	<i>x</i>	<i>y</i>	<i>z</i>
C(1)	7.520153	-1.335935	-0.057351	H(47)	-0.070975	-3.746423	-1.383606
C(2)	8.851436	-1.916614	-0.044065	H(48)	1.185252	-2.859633	-2.267388
C(3)	7.661579	0.126403	-0.030656	C(49)	-1.359283	0.184278	-0.101061
C(4)	9.817140	-0.793386	0.008643	H(50)	-1.559063	-1.971783	-0.100614
C(5)	9.112923	0.406931	0.013181	C(51)	-1.269765	2.616637	-0.103351
C(6)	11.206422	-0.755527	0.049767	C(52)	-2.699634	0.700901	-0.097214
C(7)	11.861040	0.473638	0.093604	C(53)	-2.686152	2.092475	-0.098156
C(8)	11.131550	1.677736	0.106387	C(54)	-0.977820	3.436936	-1.367113
C(9)	9.742229	1.633110	0.059490	C(55)	-0.970896	3.442492	1.155069
H(10)	11.802290	-1.655356	0.044876	S(56)	-4.267510	0.025575	-0.086882
H(11)	9.155403	2.542721	0.064995	C(57)	-3.962169	2.625533	-0.092243
O(12)	6.780091	0.963256	-0.038743	H(58)	-1.185532	2.857718	-2.269876
C(13)	9.214011	-3.245109	-0.078673	H(59)	-1.595787	4.338600	-1.384148
C(14)	8.291871	-4.323491	-0.143764	H(60)	0.070960	3.745038	-1.387009
C(15)	10.562424	-3.690316	-0.057404	H(61)	0.077906	3.750897	1.167888
F(16)	7.580532	-5.233285	-0.197765	H(62)	-1.588842	4.344181	1.171550
F(17)	11.641202	-4.105113	-0.041530	H(63)	-1.173511	2.867276	2.061548
C(18)	13.372147	0.421843	0.180859	C(64)	-4.971728	1.643896	-0.084605
C(19)	11.771046	3.048595	0.124325	H(65)	-4.207057	3.681142	-0.092323
F(20)	13.839104	-0.782584	-0.174430	C(66)	-6.325793	2.025925	-0.075587
F(21)	13.797653	0.649589	1.430877	C(67)	-7.520104	1.335881	-0.057039
F(22)	13.961646	1.317224	-0.619337	H(68)	-6.407410	3.107524	-0.080880
F(23)	12.255884	3.382080	-1.079497	C(69)	-8.851359	1.916633	-0.043622
F(24)	12.773173	3.135907	1.005877	C(70)	-7.661608	-0.126449	-0.030145
F(25)	10.877586	3.990921	0.456483	C(71)	-9.817123	0.793445	0.008830
C(26)	6.325874	-2.026060	-0.074899	C(72)	-9.213866	3.245170	-0.077438
H(27)	6.407545	-3.107662	-0.079154	C(73)	-9.112967	-0.406907	0.013524
C(28)	4.971801	-1.644078	-0.083804	O(74)	-6.780166	-0.963349	-0.038163
S(29)	4.267577	-0.025769	-0.087476	C(75)	-11.206417	0.755652	0.049657
C(30)	3.962246	-2.625734	-0.090380	C(76)	-8.291672	4.323573	-0.141391
C(31)	2.699707	-0.701106	-0.096980	C(77)	-10.562264	3.690426	-0.056144
C(32)	2.686226	-2.092691	-0.096548	C(78)	-9.742340	-1.633052	0.059778
H(33)	4.207150	-3.681339	-0.089550	C(79)	-11.861105	-0.473482	0.093382
C(34)	1.359350	-0.184495	-0.101144	H(80)	-11.802239	1.655509	0.044530
C(35)	1.269834	-2.616851	-0.101060	N(81)	-7.580293	5.233394	-0.194407
C(36)	0.491553	-1.306070	-0.101777	N(82)	-11.641033	4.105247	-0.040266
C(37)	0.876298	1.128378	-0.102745	C(83)	-11.131672	-1.677608	0.106401
C(38)	0.971079	-3.441680	1.158048	H(84)	-9.155563	-2.542694	0.065465
C(39)	0.977770	-3.438176	-1.364140	C(85)	-13.372244	-0.421635	0.180063
C(40)	-0.876225	-1.128600	-0.101432	C(86)	-11.771233	-3.048437	0.124190
C(41)	-0.491483	1.305855	-0.102973	F(87)	-13.839042	0.782754	-0.175564
H(42)	1.559153	1.971551	-0.102916	F(88)	-13.798240	-0.649201	1.429950
H(43)	1.173785	-2.865733	2.064042	F(89)	-13.961444	-1.317110	-0.620244
H(44)	-0.077722	-3.750076	1.171209	F(90)	-12.256364	-3.381614	-1.079595
H(45)	1.589009	-4.343365	1.175219	F(91)	-12.773172	-3.135898	1.005948
H(46)	1.595863	-4.339765	-1.380572	F(92)	-10.877745	-3.990879	0.455939

M ₁ (simplified model of IDIC-4CF ₃)			
Lowest Vibrational Frequencies in Chloroform			
Vibration Number	Frequency	Vibration Number	Frequency
1	4.440 cm ⁻¹	6	18.980 cm ⁻¹
2	7.990 cm ⁻¹	7	27.220 cm ⁻¹
3	8.130 cm ⁻¹	8	27.590 cm ⁻¹
4	13.590 cm ⁻¹	9	33.120 cm ⁻¹
5	14.760 cm ⁻¹	10	35.880 cm ⁻¹

The largest magnitude imaginary frequency before projecting out the vibrations and rotations was $3.7577i$ cm⁻¹.

M₂ (simplified model of IDIC-4(CH)₂)

Optimized Geometry in Chloroform

Atom (No.)	<i>x</i>	<i>y</i>	<i>z</i>	Atom (No.)	<i>x</i>	<i>y</i>	<i>z</i>
C(1)	7.594014	-0.884922	0.056250	H(47)	0.150433	-3.748331	-1.126997
C(2)	8.958424	-1.390617	0.027047	H(48)	1.342347	-2.789427	-2.024241
C(3)	7.648718	0.586560	0.013275	C(49)	-1.369337	0.099903	0.139879
C(4)	9.857478	-0.225972	-0.073701	H(50)	-1.432972	-2.064659	0.140141
C(5)	9.069426	0.955783	-0.074097	C(51)	-1.429705	2.532341	0.140758
C(6)	11.225722	-0.121835	-0.163235	C(52)	-2.739564	0.533660	0.132036
C(7)	11.825864	1.159553	-0.252822	C(53)	-2.811166	1.922177	0.131027
C(8)	11.016661	2.339942	-0.246638	C(54)	-1.178105	3.376426	-1.115783
C(9)	9.610819	2.205371	-0.154146	C(55)	-1.192814	3.368002	1.405957
H(10)	11.874820	-0.986949	-0.171355	S(56)	-4.265707	-0.234846	0.115200
H(11)	8.972136	3.082882	-0.149690	C(57)	-4.118472	2.377071	0.118528
O(12)	6.704909	1.356965	0.038767	H(58)	-1.341934	2.790460	-2.023278
C(13)	9.382955	-2.703951	0.093127	H(59)	-1.850518	4.238368	-1.134311
C(14)	8.519136	-3.823038	0.215109	H(60)	-0.150132	3.748857	-1.125355
C(15)	10.749618	-3.084077	0.056243	H(61)	-0.165117	3.740481	1.429842
N(16)	7.857583	-4.766752	0.316295	H(62)	-1.865855	4.229488	1.422543
N(17)	11.847457	-3.446791	0.029890	H(63)	-1.366959	2.775763	2.307429
C(18)	11.642856	3.603284	-0.336223	C(64)	-5.065990	1.337647	0.106583
C(19)	13.230458	1.296895	-0.351022	H(65)	-4.427110	3.415911	0.116260
C(20)	13.808193	2.538521	-0.437481	C(66)	-6.443120	1.640308	0.087868
C(21)	13.008804	3.700585	-0.429696	C(67)	-7.593989	0.884926	0.055825
H(22)	11.024799	4.495035	-0.330827	H(68)	-6.584774	2.715697	0.092515
H(23)	13.844252	0.402194	-0.357026	C(69)	-8.958402	1.390629	0.026767
H(24)	14.885943	2.630736	-0.512302	C(70)	-7.648698	-0.586550	0.012598
H(25)	13.479952	4.674769	-0.498593	C(71)	-9.857479	0.225986	-0.073793
C(26)	6.443146	-1.640316	0.088106	C(72)	-9.382926	2.703970	0.092734
H(27)	6.584808	-2.715705	0.092571	C(73)	-9.069426	-0.955767	-0.074473
C(28)	5.066013	-1.337665	0.106746	O(74)	-6.704881	-1.356957	0.037741
S(29)	4.265724	0.234827	0.115733	C(75)	-11.225750	0.121849	-0.162906
C(30)	4.118490	-2.377091	0.118180	C(76)	-8.519096	3.823089	0.214351
C(31)	2.739580	-0.533683	0.132193	C(77)	-10.749596	3.084086	0.056017
C(32)	2.811183	-1.922203	0.130696	C(78)	-9.610835	-2.205351	-0.154477
H(33)	4.427130	-3.415930	0.115621	C(79)	-11.825914	-1.159536	-0.252387
C(34)	1.369351	-0.099932	0.140028	H(80)	-11.874856	0.986960	-0.170739
C(35)	1.429721	-2.532371	0.139935	N(81)	-7.857520	4.766820	0.315227
C(36)	0.571788	-1.272172	0.141713	N(82)	-11.847447	3.446768	0.029764
C(37)	0.804582	1.180036	0.141904	C(83)	-11.016702	-2.339922	-0.246567
C(38)	1.192569	-3.368639	1.404677	H(84)	-8.972141	-3.082856	-0.150308
C(39)	1.178385	-3.375855	-1.117069	C(85)	-13.230542	-1.296880	-0.350091
C(40)	-0.804569	-1.180069	0.141342	C(86)	-11.642917	-3.603258	-0.336103
C(41)	-0.571775	1.272141	0.142128	C(87)	-13.808297	-2.538499	-0.436501
H(42)	1.432982	2.064629	0.141129	H(88)	-13.844346	-0.402184	-0.355759
H(43)	1.366526	-2.776846	2.306479	C(89)	-13.008896	-3.700558	-0.429140
H(44)	0.164867	-3.741133	1.428177	H(90)	-11.024854	-4.495006	-0.331006
H(45)	1.865600	-4.230142	1.420991	H(91)	-14.886074	-2.630715	-0.510936
H(46)	1.850851	-4.237747	-1.135893	H(92)	-13.480060	-4.674739	-0.497974

M ₂ (simplified model of IDIC-4(CH) ₂)			
Lowest Vibrational Frequencies in Chloroform			
Vibration Number	Frequency	Vibration Number	Frequency
1	1.430 cm ⁻¹	6	25.490 cm ⁻¹
2	5.240 cm ⁻¹	7	34.750 cm ⁻¹
3	10.230 cm ⁻¹	8	38.020 cm ⁻¹
4	16.800 cm ⁻¹	9	38.410 cm ⁻¹
5	18.650 cm ⁻¹	10	45.700 cm ⁻¹

The largest magnitude imaginary frequency before projecting out the vibrations and rotations was $10.6013i$ cm⁻¹.

M ₃ (simplified model of IDIC-4CN)							
Optimized Geometry in Chloroform							
Atom (No.)	<i>x</i>	<i>y</i>	<i>z</i>	Atom (No.)	<i>x</i>	<i>y</i>	<i>z</i>
C(1)	-7.593683	-0.816951	0.022905	H(43)	-0.183140	-3.742649	1.310845
C(2)	-8.959586	-1.307587	0.026822	H(44)	-1.373846	-2.772864	2.197903
C(3)	-7.634529	0.649003	-0.007058	C(45)	1.368563	0.090063	0.030230
C(4)	-9.851551	-0.124238	-0.020659	H(46)	1.418925	-2.075279	0.030177
C(5)	-9.064729	1.030428	-0.036964	C(47)	1.446235	2.523410	0.032636
C(6)	-11.235938	-0.003530	-0.049551	C(48)	2.740909	0.513012	0.029724
C(7)	-11.795178	1.275898	-0.093460	C(49)	2.823029	1.903323	0.031305
C(8)	-10.983663	2.430852	-0.106857	C(50)	1.208611	3.362839	1.295264
C(9)	-9.595540	2.301839	-0.078014	C(51)	1.207932	3.366574	-1.227369
H(10)	-11.898875	-0.856224	-0.041047	S(52)	4.258230	-0.268709	0.025851
H(11)	-8.951037	3.172369	-0.088271	C(53)	4.131500	2.347365	0.031394
O(12)	-6.700770	1.426872	-0.010742	H(54)	1.374157	2.771673	2.198999
C(13)	-9.409727	-2.608904	0.074384	H(55)	1.886749	4.220131	1.313052
C(14)	-8.560308	-3.745619	0.135262	H(56)	0.183368	3.742012	1.312656
C(15)	-10.784704	-2.963870	0.073646	H(57)	0.182648	3.745722	-1.243108
N(16)	-7.910479	-4.700393	0.186439	H(58)	1.885965	4.223993	-1.242931
N(17)	-11.889716	-3.302876	0.074896	H(59)	1.373056	2.778122	-2.132954
C(18)	-11.575007	3.726416	-0.150411	C(60)	5.071941	1.297916	0.028330
C(19)	-13.214950	1.405473	-0.125618	H(61)	4.448712	3.383533	0.034020
N(20)	-12.041667	4.780657	-0.185361	C(62)	6.447125	1.586978	0.030564
N(21)	-14.363714	1.504281	-0.151695	C(63)	7.593679	0.816937	0.022628
C(22)	-6.447146	-1.587009	0.030564	H(64)	6.602378	2.660434	0.037435
H(23)	-6.602406	-2.660466	0.037188	C(65)	8.959574	1.307590	0.026584
C(24)	-5.071962	-1.297945	0.028254	C(66)	7.634545	-0.649013	-0.007485
S(25)	-4.258266	0.268683	0.026263	C(67)	9.851559	0.124247	-0.020719
C(26)	-4.131522	-2.347391	0.030883	C(68)	9.409713	2.608918	0.073911
C(27)	-2.740937	-0.513033	0.029712	C(69)	9.064752	-1.030426	-0.037179
C(28)	-2.823052	-1.903338	0.030806	O(70)	6.700797	-1.426895	-0.011396
H(29)	-4.448724	-3.383561	0.033195	C(71)	11.235951	0.003552	-0.049314
C(30)	-1.368594	-0.090075	0.030249	C(72)	8.560295	3.745653	0.134410
C(31)	-1.446262	-2.523424	0.031684	C(73)	10.784689	2.963883	0.073206
C(32)	-0.580177	-1.269236	0.030730	C(74)	9.595581	-2.301831	-0.078112
C(33)	-0.796383	1.186711	0.030779	C(75)	11.795212	-1.275872	-0.093114
C(34)	-1.208183	-3.365922	-1.228813	H(76)	11.898880	0.856251	-0.040638
C(35)	-1.208407	-3.363528	1.293819	N(77)	7.910471	4.700450	0.185270
C(36)	0.796354	-1.186724	0.030334	N(78)	11.889707	3.302870	0.074477
C(37)	0.580149	1.269222	0.031188	C(79)	10.983711	-2.430832	-0.106678
H(38)	-1.418954	2.075267	0.030964	H(80)	8.951088	-3.172366	-0.088475
H(39)	-1.373444	-2.776980	-2.134054	C(81)	13.214993	-1.405433	-0.124986
H(40)	-0.182915	-3.745095	-1.244931	C(82)	11.575073	-3.726394	-0.150073
H(41)	-1.886251	-4.223307	-1.244713	N(83)	14.363762	-1.504230	-0.150833
H(42)	-1.886490	-4.220872	1.311252	N(84)	12.041748	-4.780633	-0.184896

M_3 (simplified model of IDIC-4CN)			
Lowest Vibrational Frequencies in Chloroform			
Vibration Number	Frequency	Vibration Number	Frequency
1	3.860 cm^{-1}	6	26.260 cm^{-1}
2	4.160 cm^{-1}	7	33.930 cm^{-1}
3	10.850 cm^{-1}	8	37.730 cm^{-1}
4	17.440 cm^{-1}	9	38.180 cm^{-1}
5	18.120 cm^{-1}	10	41.320 cm^{-1}

The largest magnitude imaginary frequency before projecting out the vibrations and rotations was $9.7885i \text{ cm}^{-1}$.

M_4 (simplified model of IDIC-2CN2COOCH3)

Optimized Geometry in Chloroform

Atom (No.)	x	y	z	Atom (No.)	x	y	z
C(1)	7.519631	1.337113	0.034520	H(48)	-0.074437	3.746708	1.337696
C(2)	8.851482	1.916545	0.030976	H(49)	1.181142	2.861152	2.223611
C(3)	7.659274	-0.125118	0.009363	C(50)	-1.359196	-0.184991	0.056642
C(4)	9.817536	0.793237	-0.013413	H(51)	-1.559972	1.970989	0.056663
C(5)	9.109046	-0.410421	-0.022903	C(52)	-1.268819	-2.617347	0.058456
C(6)	11.205429	0.757391	-0.044996	C(53)	-2.699278	-0.702012	0.054679
C(7)	11.850981	-0.485803	-0.084688	C(54)	-2.685446	-2.093672	0.055749
C(8)	11.121503	-1.690823	-0.091917	C(55)	-0.974691	-3.438609	1.321035
C(9)	9.730164	-1.640465	-0.060231	C(56)	-0.971481	-3.442014	-1.201146
H(10)	11.811788	1.651396	-0.041282	S(57)	-4.267153	-0.026843	0.048441
H(11)	9.147135	-2.552359	-0.065995	C(58)	-3.961355	-2.626894	0.053296
O(12)	6.775136	-0.959824	0.011314	H(59)	-1.181286	-2.860284	2.224627
C(13)	9.214029	3.245285	0.068249	H(60)	-1.592300	-4.340513	1.338198
C(14)	8.291234	4.323523	0.124008	H(61)	0.074228	-3.746365	1.339148
C(15)	10.562348	3.690756	0.059979	H(62)	0.077471	-3.749842	-1.215774
N(16)	7.579261	5.233267	0.170602	H(63)	-1.589025	-4.343977	-1.217445
N(17)	11.641332	4.105239	0.054882	H(64)	-1.175761	-2.866125	-2.106819
C(18)	11.833134	-3.000337	-0.135001	C(65)	-4.971284	-1.645373	0.048618
O(19)	13.031885	-3.116935	-0.167834	H(66)	-4.206113	-3.682531	0.054578
O(20)	10.982480	-4.022148	-0.133714	C(67)	-6.325285	-2.027761	0.045920
C(21)	11.577539	-5.325600	-0.177505	C(68)	-7.519629	-1.337116	0.034231
H(22)	10.746058	-6.025336	-0.167610	H(69)	-6.406742	-3.109339	0.051653
H(23)	12.166443	-5.440268	-1.088342	C(70)	-8.851472	-1.916555	0.030739
H(24)	12.218424	-5.476706	0.691919	C(71)	-7.659274	0.125109	0.008835
C(25)	13.280541	-0.440391	-0.117465	C(72)	-9.817540	-0.793245	-0.013463
N(26)	14.419719	-0.259232	-0.140797	C(73)	-9.214023	-3.245304	0.067746
C(27)	6.325299	2.027773	0.045855	C(74)	-9.109051	0.410411	-0.023204
H(28)	6.406760	3.109352	0.051227	O(75)	-6.775135	0.959817	0.010492
C(29)	4.971292	1.645386	0.048532	C(76)	-11.205439	-0.757396	-0.044653
S(30)	4.267169	0.026860	0.048963	C(77)	-8.291230	-4.323565	0.123115
C(31)	3.961371	2.626909	0.052660	C(78)	-10.562342	-3.690772	0.059470
C(32)	2.699289	0.702034	0.054760	C(79)	-9.730173	1.640454	-0.060463
C(33)	2.685458	2.093682	0.055222	C(80)	-11.850999	0.485798	-0.084274
H(34)	4.206121	3.682548	0.053491	H(81)	-11.811804	-1.651396	-0.040669
C(35)	1.359207	0.185009	0.056753	N(82)	-7.579259	-5.233329	0.169364
C(36)	1.268835	2.617367	0.057536	N(83)	-11.641329	-4.105247	0.054356
C(37)	0.490965	1.306283	0.057331	C(84)	-11.121519	1.690815	-0.091806
C(38)	0.876713	-1.128135	0.057587	H(85)	-9.147140	2.552345	-0.066423
C(39)	0.971682	3.441576	-1.202399	C(86)	-13.280569	0.440387	-0.116593
C(40)	0.974526	3.439098	1.319783	C(87)	-11.833156	3.000329	-0.134821
C(41)	-0.876702	1.128157	0.056979	N(88)	-14.419755	0.259227	-0.139531
C(42)	-0.490956	-1.306260	0.057818	O(89)	-13.031911	3.116931	-0.167467
H(43)	1.559985	-1.970968	0.057740	O(90)	-10.982498	4.022138	-0.133724
H(44)	1.176018	2.865343	-2.107841	C(91)	-11.577559	5.325590	-0.177488
H(45)	-0.077244	3.749489	-1.217268	H(92)	-10.746077	6.025325	-0.167671
H(46)	1.589297	4.343485	-1.5218959	H(93)	-12.166534	5.440246	-1.088281
H(47)	1.592011	4.341092	1.336628	H(94)	-12.218377	5.476709	0.691983

\mathbf{M}_4 (simplified model of IDIC-2CN2COOCH3)			
Lowest Vibrational Frequencies in Chloroform			
Vibration Number	Frequency	Vibration Number	Frequency
1	3.850 cm^{-1}	6	20.570 cm^{-1}
2	7.770 cm^{-1}	7	27.970 cm^{-1}
3	8.690 cm^{-1}	8	28.530 cm^{-1}
4	14.820 cm^{-1}	9	32.350 cm^{-1}
5	15.740 cm^{-1}	10	34.040 cm^{-1}

The largest magnitude imaginary frequency before projecting out the vibrations and rotations was $4.2376i \text{ cm}^{-1}$.

Optimized Geometries and Frequencies in Acetonitrile

M ₀ (simplified model of IDIC-4Cl)							
Optimized Geometry in Acetonitrile							
Atom (No.)	<i>x</i>	<i>y</i>	<i>z</i>	Atom (No.)	<i>x</i>	<i>y</i>	<i>z</i>
C(1)	-7.585660	-0.919075	0.014336	H(41)	-0.131945	-3.745730	1.258926
C(2)	-8.946001	-1.427661	0.034197	H(42)	-1.332086	-2.791811	2.151026
C(3)	-7.650889	0.549840	-0.012316	C(43)	1.367603	0.107462	-0.016583
C(4)	-9.851922	-0.258608	0.006793	H(44)	1.445293	-2.056938	-0.016564
C(5)	-9.082570	0.907616	-0.018354	C(45)	1.414363	2.541193	-0.014200
C(6)	-11.236922	-0.153620	0.003802	C(46)	2.734691	0.548984	-0.013357
C(7)	-11.814255	1.113521	-0.023501	C(47)	2.799091	1.938816	-0.011034
C(8)	-11.026029	2.272701	-0.047463	C(48)	1.162134	3.379489	1.246261
C(9)	-9.640056	2.167359	-0.044985	C(49)	1.168547	3.379863	-1.275758
H(10)	-11.891475	-1.012448	0.020826	S(50)	4.263950	-0.211529	-0.010301
H(11)	-9.016192	3.052690	-0.063546	C(51)	4.102960	2.400702	-0.004731
O(12)	-6.722865	1.336250	-0.028705	H(52)	1.332208	2.791401	2.151254
C(13)	-9.374342	-2.738293	0.078404	H(53)	1.829733	4.245011	1.264600
C(14)	-8.512762	-3.865902	0.117512	H(54)	0.132040	3.745512	1.259396
C(15)	-10.743361	-3.113038	0.094992	H(55)	0.138543	3.745899	-1.293977
N(16)	-7.860041	-4.819946	0.151631	H(56)	1.836339	4.245306	-1.290444
N(17)	-11.842223	-3.472572	0.110024	H(57)	1.343181	2.791987	-2.180018
Cl(18)	-11.744418	3.839682	-0.080702	C(58)	5.056808	1.365437	-0.002816
Cl(19)	-13.536904	1.220259	-0.027107	H(59)	4.404925	3.441351	-0.000114
C(20)	-6.430700	-1.672248	0.010583	C(60)	6.430650	1.672172	0.010459
H(21)	-6.570447	-2.747911	0.018963	C(61)	7.585641	0.919035	0.014145
C(22)	-5.056857	-1.365528	-0.002706	H(62)	6.570374	2.747836	0.018939
S(23)	-4.264005	0.211438	-0.010088	C(63)	8.945961	1.427670	0.034100
C(24)	-4.103016	-2.400793	-0.004736	C(64)	7.650931	-0.549876	-0.012633
C(25)	-2.734744	-0.549078	-0.013269	C(65)	9.851930	0.258654	0.006751
C(26)	-2.799145	-1.938903	-0.011052	C(66)	9.374277	2.738313	0.078285
H(27)	-4.404976	-3.441443	-0.000194	C(67)	9.082627	-0.907597	-0.018561
C(28)	-1.367657	-0.107552	-0.016544	O(68)	6.722945	-1.336327	-0.029175
C(29)	-1.414419	-2.541284	-0.014382	C(69)	11.236932	0.153724	0.003990
C(30)	-0.564108	-1.276202	-0.016664	C(70)	8.512682	3.865914	0.117313
C(31)	-0.811592	1.176324	-0.016901	C(71)	10.743291	3.113074	0.094907
C(32)	-1.168741	-3.379776	-1.276088	C(72)	9.640167	-2.167317	-0.045190
C(33)	-1.162058	-3.379757	1.245932	C(73)	11.814321	-1.113392	-0.023293
C(34)	0.811539	-1.176415	-0.017030	H(74)	11.891448	1.012578	0.021199
C(35)	0.564056	1.276111	-0.016565	N(75)	7.859978	4.819973	0.151357
H(36)	-1.445346	2.056847	-0.016334	N(76)	11.842156	3.472601	0.109923
H(37)	-1.343442	-2.791763	-2.180247	C(77)	11.026145	-2.272602	-0.047466
H(38)	-0.138752	-3.745848	-1.294464	H(78)	9.016341	-3.052671	-0.063900
H(39)	-1.836567	-4.245193	-1.290834	Cl(79)	13.536975	-1.220060	-0.026605
H(40)	-1.829613	-4.245314	1.264198	Cl(80)	11.744603	-3.839551	-0.080731

\mathbf{M}_0 (simplified model of IDIC-4Cl)			
Lowest Vibrational Frequencies in Acetonitrile			
Vibration Number	Frequency	Vibration Number	Frequency
1	4.720 cm^{-1}	6	23.500 cm^{-1}
2	8.280 cm^{-1}	7	33.200 cm^{-1}
3	9.790 cm^{-1}	8	37.870 cm^{-1}
4	16.010 cm^{-1}	9	38.030 cm^{-1}
5	17.760 cm^{-1}	10	38.590 cm^{-1}

The largest magnitude imaginary frequency before projecting out the vibrations and rotations was $6.9659i \text{ cm}^{-1}$.

M₁ (simplified model of IDIC-4CF₃)

Optimized Geometry in Acetonitrile

Atom (No.)	<i>x</i>	<i>y</i>	<i>z</i>	Atom (No.)	<i>x</i>	<i>y</i>	<i>z</i>
C(1)	7.520209	-1.330429	-0.067698	H(47)	-0.069776	-3.745958	-1.395265
C(2)	8.849228	-1.911726	-0.054862	H(48)	1.186924	-2.860078	-2.279811
C(3)	7.662748	0.131046	-0.034497	C(49)	-1.358913	0.183454	-0.113507
C(4)	9.816772	-0.790399	0.009187	H(50)	-1.558395	-1.972884	-0.113973
C(5)	9.114431	0.410635	0.016622	C(51)	-1.270630	2.616419	-0.114195
C(6)	11.205484	-0.755123	0.057241	C(52)	-2.699114	0.699193	-0.109319
C(7)	11.861996	0.472685	0.110069	C(53)	-2.686548	2.091474	-0.109188
C(8)	11.134381	1.677652	0.125055	C(54)	-0.979201	3.437814	-1.377415
C(9)	9.745083	1.635599	0.071574	C(55)	-0.972011	3.441635	1.144762
H(10)	11.799685	-1.655776	0.051467	S(56)	-4.266363	0.022905	-0.098980
H(11)	9.160067	2.546297	0.078600	C(57)	-3.962072	2.623862	-0.102624
O(12)	6.782608	0.969796	-0.042370	H(58)	-1.187191	2.859252	-2.280577
C(13)	9.212502	-3.240744	-0.100694	H(59)	-1.597376	4.339269	-1.392661
C(14)	8.294732	-4.321154	-0.183237	H(60)	0.069629	3.745493	-1.396543
C(15)	10.560156	-3.686818	-0.077040	H(61)	0.076787	3.749778	1.156925
N(16)	7.593459	-5.237835	-0.252622	H(62)	-1.590342	4.342964	1.160953
N(17)	11.637344	-4.106316	-0.060024	H(63)	-1.174528	2.865745	2.050874
C(18)	13.371799	0.417478	0.204579	C(64)	-4.971961	1.641361	-0.095431
C(19)	11.776118	3.046599	0.153059	H(65)	-4.206554	3.679429	-0.101909
F(20)	13.839758	-0.785862	-0.154618	C(66)	-6.324954	2.021835	-0.086721
F(21)	13.793626	0.637839	1.457859	C(67)	-7.520237	1.330514	-0.067587
F(22)	13.968783	1.315949	-0.587606	H(68)	-6.407665	3.103370	-0.091702
F(23)	12.270645	3.385497	-1.046142	C(69)	-8.849284	1.911748	-0.054658
F(24)	12.774649	3.127752	1.040780	C(70)	-7.662701	-0.130966	-0.034345
F(25)	10.884627	3.990371	0.484238	C(71)	-9.816771	0.790369	0.009300
C(26)	6.324901	-2.021714	-0.086700	C(72)	-9.212640	3.240750	-0.100325
H(27)	6.407587	-3.103250	-0.091643	C(73)	-9.114372	-0.410630	0.016709
C(28)	4.971910	-1.641219	-0.095331	O(74)	-6.782514	-0.969668	-0.042141
S(29)	4.266311	-0.022764	-0.099058	C(75)	-11.205483	0.755026	0.057270
C(30)	3.962015	-2.623720	-0.102177	C(76)	-8.294950	4.321238	-0.182783
C(31)	2.699060	-0.699051	-0.109197	C(77)	-10.560320	3.686741	-0.076569
C(32)	2.686492	-2.091335	-0.108771	C(78)	-9.744966	-1.635626	0.071592
H(33)	4.206498	-3.679287	-0.101287	C(79)	-11.861939	-0.472812	0.110068
C(34)	1.358860	-0.183312	-0.113470	H(80)	-11.799725	1.655653	0.051478
C(35)	1.270574	-2.616279	-0.113553	N(81)	-7.593770	5.237997	-0.252084
C(36)	0.491881	-1.305992	-0.114496	N(82)	-11.637539	4.106154	-0.059444
C(37)	0.875868	1.129728	-0.114610	C(83)	-11.134263	-1.677747	0.125057
C(38)	0.972063	-3.440947	1.145818	H(84)	-9.159909	-2.546298	0.078571
C(39)	0.979045	-3.438230	-1.376360	C(85)	-13.371753	-0.417684	0.204452
C(40)	-0.875921	-1.129592	-0.114386	C(86)	-11.775918	-3.046737	0.152913
C(41)	-0.491937	1.306128	-0.114769	F(87)	-13.839756	0.785568	-0.154985
H(42)	1.558337	1.973024	-0.114366	F(88)	-13.793682	-0.637855	1.457731
H(43)	1.174669	-2.864643	2.051644	F(89)	-13.968605	-1.316325	-0.587640
H(44)	-0.076738	-3.749074	1.158197	F(90)	-12.270538	-3.385474	-1.046297
H(45)	1.590401	-4.342263	1.162338	F(91)	-12.774360	-3.128102	1.040715
H(46)	1.597237	-4.339681	-1.391279	F(92)	-10.884337	-3.990505	0.483853

M_1 (simplified model of IDIC-4CF ₃)			
Lowest Vibrational Frequencies in Acetonitrile			
Vibration Number	Frequency	Vibration Number	Frequency
1	4.590 cm ⁻¹	6	18.960 cm ⁻¹
2	7.960 cm ⁻¹	7	27.230 cm ⁻¹
3	9.020 cm ⁻¹	8	27.820 cm ⁻¹
4	13.820 cm ⁻¹	9	33.460 cm ⁻¹
5	14.770 cm ⁻¹	10	35.740 cm ⁻¹

The largest magnitude imaginary frequency before projecting out the vibrations and rotations was $3.4736i$ cm⁻¹.

M₂ (simplified model of IDIC-4(CH)₂)

Optimized Geometry in Acetonitrile

Atom (No.)	<i>x</i>	<i>y</i>	<i>z</i>	Atom (No.)	<i>x</i>	<i>y</i>	<i>z</i>
C(1)	-7.592522	0.881024	0.030538	H(47)	-0.128274	3.819404	-0.906000
C(2)	-8.955193	1.387205	-0.002070	H(48)	-1.308934	2.911886	-1.876625
C(3)	-7.648312	-0.589684	-0.038215	C(49)	1.369991	-0.109085	0.165524
C(4)	-9.855196	0.224757	-0.096296	H(50)	1.433619	2.055684	0.278750
C(5)	-9.068355	-0.957957	-0.106680	C(51)	1.431295	-2.541967	0.041303
C(6)	-11.222739	0.122748	-0.157177	C(52)	2.739925	-0.532332	0.156394
C(7)	-11.834122	-1.157574	-0.237546	C(53)	2.812336	-1.921296	0.081910
C(8)	-11.026212	-2.338916	-0.260189	C(54)	1.199076	-3.303728	-1.266578
C(9)	-9.610613	-2.206492	-0.186415	C(55)	1.175758	-3.450215	1.254975
H(10)	-11.871186	0.988253	-0.146937	S(56)	4.265546	0.236782	0.190090
H(11)	-8.974540	-3.085820	-0.201319	C(57)	4.119166	-2.375688	0.056821
O(12)	-6.705070	-1.361590	-0.039517	H(58)	1.372221	-2.666129	-2.143077
C(13)	-9.380173	2.701081	0.044282	H(59)	1.871664	-4.165341	-1.326300
C(14)	-8.510513	3.830573	0.146014	H(60)	0.171095	-3.675795	-1.315367
C(15)	-10.745537	3.093603	0.012527	H(61)	0.148177	-3.822670	1.238135
N(16)	-7.858586	4.779217	0.224541	H(62)	1.849213	-4.311274	1.228374
N(17)	-11.841064	3.463746	-0.016551	H(63)	1.340395	-2.909812	2.187496
C(18)	-11.652568	-3.601362	-0.339884	C(64)	5.067122	-1.335746	0.116507
C(19)	-13.238049	-1.292802	-0.307543	H(65)	4.426970	-3.414585	0.011294
C(20)	-13.816297	-2.533801	-0.393761	C(66)	6.443291	-1.636943	0.095139
C(21)	-13.018177	-3.696724	-0.404457	C(67)	7.594987	-0.880483	0.092187
H(22)	-11.035544	-4.493720	-0.353348	H(68)	6.585843	-2.712204	0.056456
H(23)	-13.851267	-0.397760	-0.304770	C(69)	8.957683	-1.386544	0.059169
H(24)	-14.893469	-2.624739	-0.447552	C(70)	7.650767	0.590357	0.067681
H(25)	-13.489814	-4.670058	-0.471031	C(71)	9.857768	-0.223733	-0.070736
C(26)	-6.440830	1.637368	0.096223	C(72)	9.382580	-2.700670	0.161539
H(27)	-6.583369	2.712622	0.140399	C(73)	9.070883	0.958948	-0.058541
C(28)	-5.064661	1.336111	0.117416	O(74)	6.707474	1.362147	0.127858
S(29)	-4.263086	-0.236450	0.067287	C(75)	11.225412	-0.121368	-0.209844
C(30)	-4.116708	2.376016	0.200940	C(76)	8.532753	-3.810625	0.338543
C(31)	-2.737477	0.532616	0.136417	C(77)	10.747968	-3.073122	0.109783
C(32)	-2.809885	1.921590	0.205524	C(78)	9.613168	2.207759	-0.154161
H(33)	-4.424513	3.414925	0.237993	C(79)	11.816852	1.159272	-0.325716
C(34)	-1.367547	0.089351	0.145116	H(80)	11.873916	-0.986807	-0.241437
C(35)	-1.428849	2.522234	0.267059	N(81)	7.880739	-4.759701	0.493060
C(36)	-0.570759	1.262435	0.218574	N(82)	11.843494	-3.443255	0.080525
C(37)	-0.803105	-1.190841	0.085395	C(83)	11.008884	2.340555	-0.285838
C(38)	-1.213733	3.287265	1.582949	H(84)	8.977027	3.087027	-0.127343
C(39)	-1.156215	3.447180	-0.928570	C(85)	13.220894	1.294872	-0.473778
C(40)	0.805553	1.171104	0.228739	C(86)	11.635285	3.603302	-0.401366
C(41)	0.573204	-1.282175	0.095658	C(87)	13.799188	2.536160	-0.575912
H(42)	-1.431172	-2.075418	0.032835	H(88)	13.834165	0.399882	-0.492828
H(43)	-1.398719	2.644577	2.453905	C(89)	13.000999	3.699016	-0.544239
H(44)	-0.186133	3.659590	1.647411	H(90)	11.018213	4.495612	-0.372996
H(45)	-1.887134	4.148336	1.638315	H(91)	14.876448	2.627381	-0.688253
H(46)	-1.828894	4.308773	0.916358	H(92)	13.472668	4.672582	-0.627590

M ₂ (simplified model of IDIC-4(CH) ₂)			
Lowest Vibrational Frequencies in Acetonitrile			
Vibration Number	Frequency	Vibration Number	Frequency
1	4.020 cm ⁻¹	6	27.750 cm ⁻¹
2	7.190 cm ⁻¹	7	34.570 cm ⁻¹
3	17.070 cm ⁻¹	8	35.410 cm ⁻¹
4	17.800 cm ⁻¹	9	40.040 cm ⁻¹
5	19.750 cm ⁻¹	10	47.860 cm ⁻¹

The largest magnitude imaginary frequency before projecting out the vibrations and rotations was $5.4839i$ cm⁻¹.

M ₃ (simplified model of IDIC-4CN)							
Optimized Geometry in Acetonitrile							
Atom (No.)	<i>x</i>	<i>y</i>	<i>z</i>	Atom (No.)	<i>x</i>	<i>y</i>	<i>z</i>
C(1)	-7.593011	-0.812876	0.027051	H(43)	-0.183863	-3.742581	1.317509
C(2)	-8.956631	-1.304164	0.030424	H(44)	-1.375106	-2.773393	2.205039
C(3)	-7.634848	0.652298	-0.007674	C(45)	1.368068	0.089407	0.038217
C(4)	-9.850535	-0.122359	-0.025936	H(46)	1.418540	-2.076224	0.038008
C(5)	-9.065599	1.033042	-0.043988	C(47)	1.446355	2.523288	0.040053
C(6)	-11.234723	-0.004558	-0.060993	C(48)	2.740073	0.511842	0.037341
C(7)	-11.795213	1.273703	-0.112555	C(49)	2.822809	1.902852	0.038392
C(8)	-10.985551	2.429747	-0.127119	C(50)	1.209405	3.363135	1.302578
C(9)	-9.597405	2.303804	-0.092126	C(51)	1.207851	3.366272	-1.220090
H(10)	-11.896157	-0.858109	-0.052014	S(52)	4.256857	-0.270406	0.032895
H(11)	-8.954563	3.175398	-0.103210	C(53)	4.130588	2.346602	0.037648
O(12)	-6.702364	1.432073	-0.010901	H(54)	1.375384	2.772083	2.206348
C(13)	-9.407656	-2.605929	0.085993	H(55)	1.887818	4.220141	1.318945
C(14)	-8.562666	-3.744753	0.159932	H(56)	0.184075	3.741873	1.319562
C(15)	-10.781918	-2.962171	0.083084	H(57)	0.182471	3.744985	-1.234888
N(16)	-7.923629	-4.706240	0.222626	H(58)	1.886168	4.223377	-1.235145
N(17)	-11.885286	-3.307258	0.083237	H(59)	1.372769	2.777490	-2.125536
C(18)	-11.581875	3.722672	-0.178242	C(60)	5.071579	1.296449	0.034462
C(19)	-13.214827	1.402024	-0.151541	H(61)	4.447142	3.382822	0.039638
N(20)	-12.058529	4.772283	-0.219289	C(62)	6.445499	1.584256	0.036185
N(21)	-14.363382	1.502748	-0.183146	C(63)	7.593006	0.812866	0.026759
C(22)	-6.445523	-1.584285	0.036160	H(64)	6.601850	2.657568	0.043001
H(23)	-6.601882	-2.657598	0.042675	C(65)	8.956620	1.304169	0.030146
C(24)	-5.071602	-1.296475	0.034337	C(66)	7.634860	-0.652304	-0.008094
S(25)	-4.256897	0.270382	0.033344	C(67)	9.850542	0.122365	-0.026018
C(26)	-4.130611	-2.346626	0.036976	C(68)	9.407650	2.605948	0.085428
C(27)	-2.740104	-0.511862	0.037262	C(69)	9.065617	-1.033040	-0.044200
C(28)	-2.822833	-1.902863	0.037729	O(70)	6.702386	-1.432091	-0.011518
H(29)	-4.447156	-3.382849	0.038572	C(71)	11.234736	0.004569	-0.060753
C(30)	-1.368102	-0.089415	0.038208	C(72)	8.562670	3.744803	0.159005
C(31)	-1.446384	-2.523298	0.038900	C(73)	10.781913	2.962189	0.082457
C(32)	-0.580256	-1.269401	0.038570	C(74)	9.597439	-2.303801	-0.092181
C(33)	-0.796227	1.187678	0.038808	C(75)	11.795245	-1.273691	-0.112169
C(34)	-1.208086	-3.365544	-1.221775	H(76)	11.896166	0.858121	-0.051578
C(35)	-1.209218	-3.363892	1.300892	N(77)	7.923657	4.706328	0.221386
C(36)	0.796194	-1.187686	0.038306	N(78)	11.885289	3.307249	0.082532
C(37)	0.580225	1.269392	0.039124	C(79)	10.985593	-2.429737	-0.126888
H(38)	-1.418574	2.076216	0.038903	H(80)	8.954603	-3.175398	-0.103367
H(39)	-1.373135	-2.776226	-2.126846	C(81)	13.214867	-1.402003	-0.150847
H(40)	-0.182718	-3.744272	-1.236955	C(82)	11.581932	-3.722662	-0.177833
H(41)	-1.886427	-4.222623	-1.237222	N(83)	14.363430	-1.502721	-0.182214
H(42)	-1.887578	-4.220951	1.316843	N(84)	12.058600	-4.772273	-0.218728

M_3 (simplified model of IDIC-4CN)			
Lowest Vibrational Frequencies in Acetonitrile			
Vibration Number	Frequency	Vibration Number	Frequency
1	3.620 cm^{-1}	6	26.320 cm^{-1}
2	4.360 cm^{-1}	7	34.040 cm^{-1}
3	12.600 cm^{-1}	8	37.380 cm^{-1}
4	18.140 cm^{-1}	9	37.670 cm^{-1}
5	18.380 cm^{-1}	10	41.820 cm^{-1}

The largest magnitude imaginary frequency before projecting out the vibrations and rotations was $10.4223i \text{ cm}^{-1}$.

M₄ (simplified model of IDIC-2CN2COOCH₃)

Optimized Geometry in Acetonitrile

Atom (No.)	<i>x</i>	<i>y</i>	<i>z</i>	Atom (No.)	<i>x</i>	<i>y</i>	<i>z</i>
C(1)	7.518901	1.332940	0.044240	H(48)	-0.073853	3.746005	1.355334
C(2)	8.848337	1.912808	0.039040	H(49)	1.182791	2.861290	2.241146
C(3)	7.659352	-0.128301	0.011772	C(50)	-1.358617	-0.184475	0.074289
C(4)	9.816149	0.791310	-0.018627	H(51)	-1.559974	1.971731	0.074760
C(5)	9.109629	-0.413013	-0.030413	C(52)	-1.268685	-2.617488	0.075074
C(6)	11.203505	0.757791	-0.059335	C(53)	-2.698316	-0.700984	0.071557
C(7)	11.849810	-0.484480	-0.110096	C(54)	-2.685004	-2.093477	0.071792
C(8)	11.122785	-1.690497	-0.119077	C(55)	-0.975293	-3.439284	1.337537
C(9)	9.731569	-1.642183	-0.078198	C(56)	-0.970847	-3.441855	-1.184670
H(10)	11.808420	1.652520	-0.054796	S(57)	-4.265552	-0.025125	0.064015
H(11)	9.150054	-2.554990	-0.085264	C(58)	-3.960181	-2.626275	0.067833
O(12)	6.776788	-0.965018	0.014574	H(59)	-1.182704	-2.861365	2.241242
C(13)	9.212033	3.242024	0.087224	H(60)	-1.592795	-4.341190	1.352970
C(14)	8.294040	4.322631	0.162447	H(61)	0.073768	-3.746248	1.355369
C(15)	10.559789	3.687666	0.074019	H(62)	0.078223	-3.749005	-1.198153
N(16)	7.592534	5.239594	0.226013	H(63)	-1.588391	-4.343721	-1.200506
N(17)	11.637616	4.105794	0.065519	H(64)	-1.174949	-2.865721	-2.090264
C(18)	11.836376	-2.998343	-0.174029	C(65)	-4.970761	-1.643992	0.062625
O(19)	13.036633	-3.110155	-0.215937	H(66)	-4.204309	-3.681923	0.068233
O(20)	10.989919	-4.020621	-0.172453	C(67)	-6.323418	-2.024988	0.058648
C(21)	11.583644	-5.325126	-0.228379	C(68)	-7.518913	-1.332951	0.044245
H(22)	10.751459	-6.023663	-0.215864	H(69)	-6.406011	-3.106505	0.064356
H(23)	12.163952	-5.434824	-1.145178	C(70)	-8.848351	-1.912803	0.039021
H(24)	12.230098	-5.481540	0.635798	C(71)	-7.659343	0.128287	0.011674
C(25)	13.278987	-0.436599	-0.152189	C(72)	-9.816155	-0.791292	-0.018628
N(26)	14.417863	-0.253349	-0.182173	C(73)	-9.212083	-3.242016	0.087134
C(27)	6.323408	2.024965	0.058595	C(74)	-9.109618	0.413018	-0.030494
H(28)	6.405986	3.106483	0.064288	O(75)	-6.776769	0.964996	0.014395
C(29)	4.970748	1.643954	0.062578	C(76)	-11.203513	-0.757749	-0.059183
S(30)	4.265558	0.025087	0.064131	C(77)	-8.294122	-4.322641	0.162517
C(31)	3.960173	2.626230	0.067753	C(78)	-10.559842	-3.687634	0.073662
C(32)	2.698311	0.700939	0.071566	C(79)	-9.731536	1.642199	-0.078261
C(33)	2.684995	2.093419	0.071719	C(80)	-11.849798	0.484532	-0.109973
H(34)	4.204283	3.681881	0.068057	H(81)	-11.808448	-1.652464	-0.054502
C(35)	1.358610	0.184424	0.074303	N(82)	-7.592648	-5.239617	0.226224
C(36)	1.268680	2.617437	0.074960	N(83)	-11.637678	-4.105735	0.064918
C(37)	0.490856	1.306577	0.075161	C(84)	-11.122754	1.690536	-0.119076
C(38)	0.876740	-1.129103	0.075058	H(85)	-9.150002	2.554993	-0.085356
C(39)	0.970883	3.441850	-1.184741	C(86)	-13.278981	0.436677	-0.151893
C(40)	0.975250	3.439199	1.337466	C(87)	-11.836322	2.998393	-0.174066
C(41)	-0.876748	1.129054	0.074978	N(88)	-14.417865	0.253446	-0.181718
C(42)	-0.490864	-1.306627	0.075235	O(89)	-13.036575	3.110227	-0.216026
H(43)	1.559972	-1.971778	0.074911	O(90)	-10.989848	4.020658	-0.172427
H(44)	1.174936	2.865745	-2.090367	C(91)	-11.583548	5.325173	-0.228374
H(45)	-0.078161	3.749100	-1.198232	H(92)	-10.751358	6.023701	-0.215643
H(46)	1.588494	4.343670	-2.005500	H(93)	-12.163666	5.434943	-1.145285
H(47)	1.592634	4.341186	1.352867	H(94)	-12.230175	5.481531	0.635683

M ₄ (simplified model of IDIC-2CN2COOCH ₃)			
Lowest Vibrational Frequencies in Acetonitrile			
Vibration Number	Frequency	Vibration Number	Frequency
1	4.370 cm ⁻¹	6	20.940 cm ⁻¹
2	7.880 cm ⁻¹	7	28.480 cm ⁻¹
3	9.880 cm ⁻¹	8	28.620 cm ⁻¹
4	15.300 cm ⁻¹	10	35.650 cm ⁻¹
5	15.680 cm ⁻¹	9	33.300 cm ⁻¹

The largest magnitude imaginary frequency before projecting out the vibrations and rotations was $3.2520i$ cm⁻¹.

4 FMO theory diagram

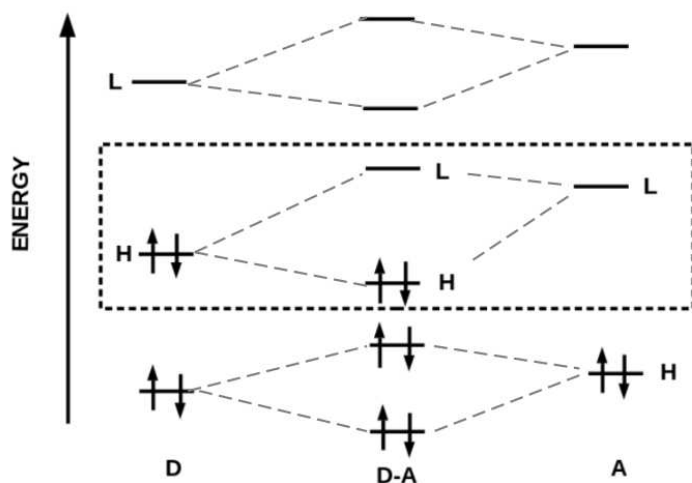


Figure 2: Generic FMO theory diagram^{16,17} with donor D and acceptor A joining to form a new D-A molecule. H indicates the HOMO level and L indicates the LUMO level. Adding an acceptor to D decreases the LUMO energy of D-A more than it decreases the HOMO energy. Adding a donor to A increases the HOMO energy of D-A more than it increases the LUMO energy.

The electronegativity of chlorine makes chloro groups electron acceptors by induction (-I, σ -acceptor). The presence of *p*-electrons may also make chloro groups electron donors by resonance (+M, π -donor). Going from IDIC to IDIC-4Cl lowers both the CV HOMO and the CV LUMO energies. According to FMO theory (**Fig. 2**), this means that the +M effect is more important than the -I effect as is usually the case. FMO theory also seems to suggest that the CV HOMO-LUMO gap should decrease on adding either an electron acceptor or an electron donor. In this case, we see that adding chloro groups has decreased the CV HOMO-LUMO gap. ±I, ±M

5 Spectral Shift

X	$\lambda_{\max}^{\text{soln}}$	$\lambda_{\max}^{\text{film}}$	red shift	Reference
IDIC(X)				
tetrakis(4-hexylphenyl)	647 nm	682 nm	0.098 eV	12
tetraoctyl	660 nm	710 nm	0.156 eV	11
tetrahexyl	670 nm	720 nm	0.129 eV	10
IDIC(X)-4Cl				
tetrakis(4-hexylphenyl)	669 nm	709 nm	0.105 eV	12
tetraoctyl	700 nm	760 nm	0.140 eV	14
tetraoctyl	690 nm	760 nm	0.165 eV	15
tetraoctyl	690 nm	760 nm	0.165 eV	11
tetrahexyl	690 nm	760 nm	0.165 eV	13

This table shows the red shift of the main peak in the absorption spectra in going from chloroform solution to thin film. The X in IDIC(X) and in IDIC(X)-4Cl is chosen to control aggregation which is one of the many parameters which may be important in organic solar cells. This aggregation is even more important when thin films are formed. A larger energy shift is expected to correspond to closer approach of the planar polycyclic core of the molecules. Interestingly, but not unexpectedly, this shift is smallest when X is largest — that is for IDIC(tetrakis(4-hexylphenyl)) and for IDIC(tetrakis(4-hexylphenyl))-4Cl.

References

- [1] Scharber, M. C., *Adv. Mater.*, 2016, **28**, 1994.
- [2] Scharber, M. C.; Muehlbacher, D.; Koppe, M.; Denk, P.; Waldouf, C.; Heeger, A. J. and Brabec, C. J., *Adv. Mater.*, 2006, **18**, 789.
- [3] Magero, D.; Mestiri, T.; Alimi, K. and Casida, M. E. In *Green Chemistry and Computational Chemistry: Shared Lessons in Sustainability*, Mammino, L., Ed.; Elsevier, 2022; page 115.
- [4] Shockley, W. and Queisser, H. J., *J. Appl. Phys.*, 1961, **32**, 510.
- [5] Frisch, M. J.; Trucks, G. W.; Schlegel, H. B.; Scuseria, G. E.; Robb, M. A.; Cheeseman, J. R.; Scalmani, G.; Barone, V.; Mennucci, B.; Petersson, G. A.; Nakatsuji, H.; Caricato, M.; Li, X.; Hratchian, H. P.; Izmaylov, A. F.; Bloino, J.; Zheng, G.; Sonnenberg, J. L.; Hada, M.; Ehara, M.; Toyota, K.; Fukuda, R.; Hasegawa, J.; Ishida, M.; Nakajima, T.; Honda, Y.; Kitao, O.; Nakai, H.; Vreven, T.; Montgomery, Jr., J. A.; Peralta, J. E.; Ogliaro, F.; Bearpark, M.; Heyd, J. J.; Brothers, E.; Kudin, K. N.; Staroverov, V. N.; Kobayashi, R.; Normand, J.; Raghavachari, K.; Rendell, A.; Burant, J. C.; Iyengar, S. S.; Tomasi, J.; Cossi, M.; Rega, N.; Millam, J. M.; Klene, M.; Knox, J. E.; Cross, J. B.; Bakken, V.; Adamo, C.; Jaramillo, J.; Gomperts, R.; Stratmann, R. E.; Yazyev, O.; Austin, A. J.; Cammi, R.; Pomelli, C.; Ochterski, J. W.; Martin, R. L.; Morokuma, K.; Zakrzewski, V. G.; Voth, G. A.; Salvador, P.;

Dannenberg, J. J.; Dapprich, S.; Daniels, A. D.; Farkas, O.; Foresman, J. B.; Ortiz, J. V.; Cioslowski, J. and Fox, D. J., GAUSSIAN 09 Revision D.01, 2009.

- [6] Beal, R. *Morphology and Efficiency of Polymer:Fullerene Solar Cells* PhD thesis, Oxford University, 2010.
- [7] He, Y. and Li, Y., *Phys. Chem. Chem. Phys.*, 2011, **13**, 1970.
- [8] Alharbi, F. H.; Rashkeev, S. N.; El-Mellouhi, F.; Lüthi, H. P.; Tabet, N. and Kais, S., *npj Comput. Mater.*, 2015, **1**, 15003.
- [9] Reference air mass 1.5 spectra <https://www.nrel.gov/grid/solar-resource/spectra-am1.5.html>.
- [10] Lin, Y.; He, Q.; Zhao, F.; Huo, L.; Mai, J.; Lu, X. and ..., , *J. Am. Chem. Soc.*, 2016, **138**, 2973.
- [11] Huang, Z.; Zhou, R.; Lv, M.; Zhang, H.; Yang, C.; Shi, Y.; Tang, Y.; Zhang, J.; Lu, K. and Wei, Z., *Mater. Chem. Front.*, 2021, **5**, 1405.
- [12] Qu, J.; Chen, H.; Zhou, J.; Lai, H.; Liu, T.; Chao, P.; Li, D.; Xie, Z.; He, F. and Ma, Y., *ACS Appl. Mater. Interfaces*, 2018, **10**, 39992.
- [13] Li, X.; Meng, H.; Shen, F.; Su, D.; Huo, S.; Shan, J.; Huang, J. and Zhana, C., *Dyes Pigm.*, 2019, **166**, 196.
- [14] Wu, Q.; Deng, D.; Zhou, R.; Zhang, J.; Zou, W.; Liu, L.; Wu, S.; Lu, K. and Wei, Z., *ACS Appl. Mater. Interfaces*, 2020, **12**, 25100.
- [15] Zhang, Z.; Wu, Q.; Deng, D.; Zhang, J. and Wei, Z., *J. Mater. Chem. C*, 2020, **8**, 15385.
- [16] Fleming, I., *Frontier Orbitals and Organic Chemical Reactions*, John Wiley and Sons, New York, 1976.
- [17] Anh, N. T., *Frontier Orbitals: A Practical Manual*, John Wiley and Sons, The Atrium, Southern Gate, Chichester, West Sussex PO19 8SQ, England, 2007.